

# Explicit centre manifold reduction and full bifurcation analysis for an astigmatic Maxwell-Bloch laser

D.R.J.Chillingworth<sup>a</sup> G.D'Alessandro<sup>a</sup> F.Papoff<sup>b</sup>

<sup>a</sup>*Department of Mathematics, University of Southampton,  
Southampton SO17 1BJ, England, UK*

<sup>b</sup>*Department of Physics and Applied Physics, University of Strathclyde,  
107 Rottenrow, Glasgow G4 0NG, Scotland, UK*

---

## Abstract

We set up a general framework to study the bifurcations of nearly degenerate modes of a Maxwell-Bloch laser model, and we apply it specifically to the study of interactions of two modes of a laser with broken circular symmetry. We use an explicit centre manifold reduction to analyse the behaviour of this laser. Complex bifurcation sequences involving single mode solutions, mode locking and mode beating regimes are predicted. These sequences are organized by a Hopf bifurcation with  $1 : 1$  resonance and a  $Z_2$ -symmetric Takens-Bogdanov bifurcation. Numerical simulations of the original system show good agreement with theory.

*Key words:* Centre manifold, Spatial patterns in nonlinear optics, Symmetric bifurcation theory, Takens-Bogdanov, Maxwell-Bloch lasers

*PACS:* 02.30.Oz, 42.55.Ah, 42.60.Mi, 42.65.Sf, 05.45.-a

---

## 1 Introduction

Symmetries pose considerable constraints on the configuration of stationary solutions and on the time evolution of dynamical systems as well as on their bifurcation behaviour [1–4], to the extent that the presence of symmetries can often dictate the existence of certain solution branches independently of the specific model under consideration. These ideas have been fruitfully used in optics either to classify the patterns produced by experiments [5] or by models [6–8], and to infer from these the symmetry of the systems under investigation. They have also been used to study in great detail the structure of the bifurcations of normal form equations with the same symmetry as the experiments [9–11]. Despite the considerable success of these approaches, there are several limitations. In the first case, the comparison between theory and experiments is qualitative and the bifurcation diagram is not fully explored. In the second case, there is no relation between the

parameters used in the normal form analysis and the physical parameters and, furthermore, it is impossible to find where the normal forms cease to be a good approximation of the system studied. A popular alternative is to ignore symmetry altogether and to study models, usually nonlinear partial or integro-differential equations, that are derived from first principles. An advantage of this approach is that such models can be valid both close to and far from the first instability. A disadvantage is that most of the analysis has to be performed numerically, which means in practice that the bifurcation diagram is rarely analysed completely.

In this paper we derive normal form equations for a laser model in the presence of a typical breaking of cylindrical symmetry of the cavity. We then study in detail the case in which the symmetry is broken by astigmatism. In this way we are able to reduce a partial differential model to a system of ordinary differential equations and to take full advantage of the symmetry in the study of the bifurcation diagram without losing the physical meaning of the control parameters. Furthermore, we are able to find the range of the control parameters in which the normal form is in quantitative agreement with the full model and where the agreement is only qualitative. In the example discussed in this paper, we show that the normal forms predict the correct bifurcation structure and amplitude of the solutions for small values of the control parameter; for larger values only the nature of the bifurcation points is determined (see Figure 9). The bifurcations turn out to be organised by a  $Z_2$ -symmetric Takens-Bogdanov point and by a resonant Hopf bifurcation. A Takens-Bogdanov bifurcation commonly occurs in this type of problem (see [12,13], for example) and the bifurcation diagrams in [14] sketch some key features of associated branching behaviour, but here we provide a complete picture with the full state diagram (bifurcation set with associated phase portraits) for the normal form of our equations for a wide range of physically significant parameters.

The rest of this paper is organised as follows. In the next section we introduce a specific laser model, namely the Maxwell-Bloch two-level laser [15], and carry out an explicit centre manifold reduction at the first bifurcation from the trivial solution as the pump parameter is increased. We then in Section 3 look more closely at the particular case of astigmatic symmetry-breaking from geometric  $O(2)$  symmetry to  $D_2$  symmetry. The additional  $S^1$  phase-shift yields a bifurcation problem with broken  $O(2) \times S^1$  symmetry, much studied in the literature [3,14,16,17]. We find, however, that the thorough analysis of responses to linear symmetry-breaking perturbations given in [14], the treatment most relevant to our problem, does not cover all important cases as it assumes the equivalent of nonzero detuning (see Section 3) that may not hold in this problem. For the zero detuning case we use the normal form for Hopf bifurcation with 1 : 1 resonance [18], and note here how a nonlinear coordinate change converts the problem again into one with  $O(2) \times S^1$  symmetry, but now with the roles of  $SO(2)$ , the group of spatial rotation, and  $S^1$  interchanged. This has interesting implications for the interpretation of periodic solutions in terms of standing or travelling waves.

Finally, we compare the results with numerical simulations for the original problem.

## 2 Laser normal forms in the presence of generic symmetry breaking

We assume that the laser under study is a ring cavity gas laser with approximate cylindrical symmetry as shown schematically in Figure 8. This is roughly the same type of laser as used in the experiments of Reference [5] and it has also been used in many other experimental [19–26] and theoretical [10,27–30] studies of pattern formation in lasers. We use here a standard model for such a system [28], incorporating a number of assumptions.

First we assume that the light is linearly polarised and that the active medium is isotropic, so that the electric field amplitude  $\hat{F}$  can be represented by a scalar field.

Secondly we assume that the active medium can be represented as a collection of two-level atoms (Maxwell-Bloch two-level laser), *i.e.* that only two atomic levels are involved in the lasing process: this allows us to use only two functions to represent the atomic medium, namely the polarisation and the population inversion. The polarisation  $\hat{P}$  represents the induced polarisation field of the atoms, while the population inversion  $N$  measures the difference in population between the excited and the ground states.

Thirdly we assume that either the laser is producing a continuous wave of light or, if it is pulsed, that the pulses are long compared to the light period. In this case we can write the polarisation and the electric field as the product of a rapidly varying phase term and a slowly varying amplitude:

$$\hat{F}(x, y, z, t) = \frac{1}{2} \left[ F(x, y, z, t) e^{i(k_A z - \omega_A t)} + \text{c.c.} \right] \quad (1)$$

$$\hat{P}(x, y, z, t) = \frac{1}{2} \left[ P(x, y, z, t) e^{i(k_A z - \omega_A t)} + \text{c.c.} \right], \quad (2)$$

where  $\omega_A = ck_A$  is the frequency of the atomic transition, with  $c$  the speed of light and  $k_A$  the corresponding wavenumber. The amplitudes  $F$  and  $P$  are assumed to be varying much more slowly than  $\omega_A$  (slowly varying approximation) so that the second derivatives of  $F$  and  $P$  with respect to  $z$  and  $t$  in Maxwell's wave equation can be neglected with respect to their first derivatives [31].

Finally, we assume that the gain and losses per cavity round trip are small. This allows us to neglect the variation of the electric field amplitude  $F$  and of the atomic variables  $P$  and  $N$  along the cavity axis, so that the problem is reduced to two spatial dimensions (*i.e.* the centre plane of the active medium) and time.

Under these hypotheses, we can write the equations for the model as [28]

$$\frac{\partial F}{\partial t} = \mathcal{L}F + P, \quad (3)$$

$$\frac{\partial P}{\partial t} = -P + \chi F + FN, \quad (4)$$

$$\frac{\partial N}{\partial t} = -\gamma \left[ N + \frac{1}{2} (F\bar{P} + \bar{F}P) \right], \quad (5)$$

where the over-bar symbol indicates complex conjugate. The linear operator  $\mathcal{L}$  is usually a partial differential operator which depends upon the laser cavity and it is related to the propagation in the empty cavity, *i.e.* the cavity without the active medium [28]. In these equations time  $t$  is non-dimensional and is in units of the polarisation decay time. For a very large class of cavities, called *stable* in laser physics, the electric field remains confined within the cavity. For these cavities, the operator  $\mathcal{L}$  has a system of eigenfunctions  $A_n(x, y)$

$$\mathcal{L}A_n(x, y) = \beta_n A_n(x, y), \quad (6)$$

which form an orthonormal basis for the space  $\mathcal{H}$  of  $L_2$  complex functions defined in the transverse plane. The lasers we consider here are in this class. The functions  $A_n(x, y)$  are called *empty cavity modes* because they are also eigenfunctions of the operator  $\mathcal{R}_C$  that propagates the field once around the empty cavity from  $z = 0$  back to itself, namely

$$\mathcal{R}_C A_n(x, y, 0) = e^{\mu_n} A_n(x, y, 0). \quad (7)$$

The complex coefficient  $\beta_n$  represents the attenuation and phase shift of the mode  $n$  per unit time. It is related to the eigenvalue of the mode given in (7) by the relation  $\beta_n = \mu_n/T_c + i\hat{\delta}$ , where  $T_c$  is the cavity round trip time and  $\hat{\delta}$  is a detuning parameter,

$$\hat{\delta} = \omega_A - \omega_C. \quad (8)$$

Here  $\omega_C$  is a reference frequency with respect to which the propagation phase shifts of the modes are measured. The case in which  $\mathcal{L}$  is an integral operator can be dealt with in the same way, but the previous relations are slightly different.

The energy fed into the laser is represented by the pump parameter  $\chi = \chi(x, y)$  and the decay rate of the population inversion is given by  $\gamma$ . In all that follows we assume that  $\chi$  is space-independent. The appropriate calculations for a space-dependent pump are sketched in Appendix B.

Equations (3-5) have a trivial solution  $F = P = N = 0$  that is stable for sufficiently small positive values of  $\chi$ : if too little energy is provided the laser remains switched off. The linear stability of the trivial solution with respect to a small perturbation  $(\tilde{F}, \tilde{P}, \tilde{N})$  is given by

$$\frac{\partial}{\partial t} \begin{pmatrix} \tilde{F} \\ \tilde{P} \\ \tilde{N} \end{pmatrix} = \begin{pmatrix} \mathcal{L} & 1 & 0 \\ \chi & -1 & 0 \\ 0 & 0 & -\gamma \end{pmatrix} \begin{pmatrix} \tilde{F} \\ \tilde{P} \\ \tilde{N} \end{pmatrix} \quad (9)$$

and depends also on the perturbation itself. However, one can see that  $\tilde{N}$  is decoupled from  $\tilde{F}, \tilde{P}$  and it is always damped. It is convenient to expand both  $\tilde{F}$  and  $\tilde{P}$  in terms of the eigenfunctions  $A_n$  of  $\mathcal{L}$ . By projecting the equations for  $\tilde{F}$  and  $\tilde{P}$  onto the  $A_n$ , we obtain an infinite block-diagonal matrix with blocks of dimension two. The eigenvalues of these blocks are given by

$$\lambda_n = \frac{1}{2} \left[ -1 + \beta_n \pm \sqrt{(1 + \beta_n)^2 + 4\chi} \right] \quad (10)$$

and the corresponding eigenvectors are

$$\mathbf{u}_n = \frac{1}{\mathcal{N}_n} \begin{pmatrix} 1 + \lambda_n \\ \chi \\ 0 \end{pmatrix} A_n(x, y) \quad (11)$$

where  $\mathcal{N}_n$  is a normalisation factor chosen so that  $(\mathbf{v}_n, \mathbf{u}_n) = 1$ . Here  $\mathbf{v}_n$  is the corresponding eigenvector of the adjoint matrix,

$$\mathbf{v}_n = \frac{1}{\mathcal{N}_n} \begin{pmatrix} 1 + \bar{\lambda}_n \\ 1 \\ 0 \end{pmatrix} A_n(x, y), \quad (12)$$

and the inner product is defined by

$$(\mathbf{v}, \mathbf{u}) = \int \bar{\mathbf{v}}^T \mathbf{u} \, dx dy. \quad (13)$$

We have, therefore, that

$$\mathcal{N}_n^2 = (1 + \lambda_n)^2 + \chi. \quad (14)$$

From equation (10) we can calculate that the trivial solution loses its stability through a Hopf bifurcation of frequency

$$\omega_{\hat{n}} = -\frac{\Im(\beta_{\hat{n}})}{1 - \Re(\beta_{\hat{n}})} \quad (15)$$

when  $\chi = \chi_0(\hat{n})$ , where

$$\chi_0(n) = -\Re(\beta_n) (1 + \omega_n^2). \quad (16)$$

The index  $\hat{n}$  is defined as an element of the set  $\mathcal{J} \subset \mathbb{N}$  of those values of  $n$  that minimise  $\chi_0(n)$  over all the integers.

In the presence of unperturbed symmetry there may be degenerate eigenvalues. In other words, the set  $\mathcal{J}$  has more than one element. Eigenvectors corresponding to eigenvalues  $\lambda_n, n \in \mathcal{J}$  are called *active modes*. In general, we can assume that the number  $M$  of elements of  $\mathcal{J}$  is finite, in which case we say that the unperturbed system has degeneracy  $M$ : all the active modes have eigenvalue with zero real part and imaginary part given by (15). All the other modes have eigenvalue with negative real part. If the system is slightly perturbed the degeneracy is either partially or totally lifted and the eigenvalues of the active modes are no longer all equal. However, we assume that the perturbation is sufficiently small and that  $\chi$  is sufficiently close to  $\chi_0(\hat{n})$  to ensure that

$$\Re(\lambda_n) < 0 \quad \forall n \notin \mathcal{J}. \quad (17)$$

In other words, the modes that do not belong to the set  $\mathcal{J}$  are still linearly damped. We can separate the field  $\mathbf{u} = (F, P, N)^T$  into components along the space spanned by the active modes and its orthogonal complement:

$$\mathbf{u} = \sum_{n \in \mathcal{J}} f_n \mathbf{u}_n + \mathbf{u}_\perp, \quad (18)$$

where  $\mathbf{u}_\perp \equiv (F_\perp, P_\perp, N)^T$  is defined by

$$(\mathbf{v}_n, \mathbf{u}_\perp) = 0, \quad \forall n \in \mathcal{J}. \quad (19)$$

The equations for the dynamics of the active modes can be obtained by a centre manifold reduction [32] of equations (3-5). The nonlinearities in these latter equations are quadratic. As a consequence, the centre manifold reduction is greatly simplified and the equations for the active modes can be obtained up to third order by “simply” projecting the equations (3-5) onto the active modes:

$$\frac{d}{dt} f_n = \left( \mathbf{v}_n, \frac{d\mathbf{u}}{dt} \right), \quad n \in \mathcal{J}. \quad (20)$$

After rather lengthy calculations (detailed in Appendix A) we obtain that the amplitudes of the active modes are given by

$$\frac{d}{dt} f_n = \lambda_n f_n - \chi \sum_{p,j,k \in \mathcal{J}} B_{npj k} (A_n, A_j \bar{A}_k A_p) f_j \bar{f}_k f_p, \quad n \in \mathcal{J} \quad (21)$$

where

$$B_{npj k} = \frac{(1 + \lambda_p)[1 + (\lambda_j + \bar{\lambda}_k)/2]}{[1 + (\lambda_j + \bar{\lambda}_k)/\gamma] \mathcal{N}_n \mathcal{N}_p \mathcal{N}_j \mathcal{N}_k}. \quad (22)$$

### 3 Two modes and $D_2$ geometrical symmetry: an example

#### 3.1 Introduction

Equation (21) is very general: it can be used to describe the bifurcation structure of a mean field limit two level Maxwell-Bloch laser at an eigenvalue of arbitrary (finite) multiplicity. The methods used in deriving it are also completely general. However, the great advantage of using a two level Maxwell-Bloch laser model is that the nonlinear terms are relatively simple and hence the centre manifold reduction of the laser equations contains fairly few and manageable terms.

In order to illustrate the use of equation (21) we consider in this section a particularly simple case: we assume that the perfectly symmetric laser has two degenerate modes at threshold and that symmetry breaking, for example as caused by astigmatism, reduces the geometrical symmetry from  $O(2)$  to  $D_2$  and lifts the degeneracy by changing the mode resonance frequency. The geometrical symmetry of the astigmatic cavity is combined with

the phase invariance  $S^1$ - symmetry of the laser equations to give the symmetry group  $Z_2 \times S^1$  (see below). This problem has been studied in depth by many authors [14,16,17]. Dangelmayr and Knobloch [14] have provided a fairly comprehensive analysis of all the possible bifurcation scenarios induced by the symmetry breaking from  $O(2) \times S^1$  to  $Z_2 \times S^1$  in a generic system in normal form. In the laser context, various authors [9,10,29,33–35] have studied the effect of symmetry breaking on mode interactions for simple laser modes. In a similar vein, Vladimirov [36] studies the interaction between longitudinal modes in a bidirectional ring laser.

This section contributes to these studies by highlighting the fact that the two interacting modes need not be standard Gauss-Hermite modes but can be any cavity mode: for example they could be the modes of a waveguide cavity as studied in [6–8]. Moreover, we include in our analysis a bifurcation scenario with unexpected additional symmetry that is excluded from the generic studies in [14] and which arises when the frequency  $\omega_C$  of the unperturbed cavity mode and the frequency  $\omega_A$  of atomic transmission coincide. We now explain this in more detail.

Perturbations that break the symmetry typically cause the two modes to have slightly different frequencies. By a suitable choice of reference frequency we can write their coefficients  $\beta_n$  as

$$\beta_n = \kappa \{-1 + i[\delta + (-1)^n \eta]\} \quad n = 1, 2 \quad (23)$$

where  $\kappa$  is the mode amplitude decay rate and  $\delta = \hat{\delta}/\kappa$  is the scaled cavity-atom detuning parameter. We have relabelled the modes so that the two active modes have indices 1 and 2 and we have changed the reference frequency so that the active modes have frequencies  $\kappa(\delta \pm \eta)$ . In this notation  $\eta$  plays the role of symmetry breaking parameter: if  $\eta = 0$  the two modes are degenerate and the system undergoes a standard  $O(2) \times S^1$  symmetric Hopf bifurcation. If  $\delta = \pm\eta$  then atomic transition is resonant with mode  $n = 1$  and  $n = 2$  respectively. The mode with frequency closest to the atomic frequency (so that  $\Im(\beta_n)$  is closest to zero) is the first to become unstable as the pump parameter is increased from below to above threshold. However, if the atomic frequency is exactly in between those of the two modes, *i.e.* if  $\delta = 0$ , then the laser has no criterion by which to choose the most unstable mode and like Buridan’s ass does not know what to do. Unlike the unfortunate animal, though, it does not die of hunger but exhibits dynamical behaviour that is an interesting “combination” of features of the dynamics observed for  $\delta$  small and nonzero.

### 3.2 Centre Manifold Equations

We write the pump parameter  $\chi$  as

$$\chi = \kappa(1 + \varepsilon). \quad (24)$$

From (23) and (10) we see that at resonance  $\delta = \pm\eta$  the threshold value of the pump parameter is  $\chi = \kappa$ , that is  $\varepsilon = 0$ . The assumption of being close to threshold therefore becomes that  $\varepsilon$  is a small parameter. Moreover, we assume also  $|\delta \pm \eta| \ll 1$ . To write the

equations for the two modal amplitudes we simplify (21) by first expanding the coefficient of the linear term up to first order in  $\varepsilon$  and up to second order in  $\delta \pm \eta$ :

$$\lambda_n = \mu\varepsilon - \mu^3[\delta + (-1)^n\eta]^2 + i\mu[\delta + (-1)^n\eta] + \dots \quad (25)$$

where

$$\mu \equiv \frac{\kappa}{1 + \kappa}. \quad (26)$$

This expansion ensures that we keep track of all the physically relevant features of the model: in particular, the second order term in  $\delta \pm \eta$  is responsible for making the threshold value of the pump parameter dependent on the detuning. We also expand the coefficients of the nonlinear terms, but only up to order zero. In this limit equation (21) reduces to

$$\begin{aligned} \frac{d}{dt}f_n &= \mu \left\{ \varepsilon - \mu^2 [\delta + (-1)^n\eta]^2 + i[\delta + (-1)^n\eta] \right\} f_n \\ &\quad - \frac{\mu}{1 + \kappa} \sum_{j,k,p=1}^2 (A_n, A_j \bar{A}_k A_p) f_j \bar{f}_k f_p, \quad n = 1, 2. \end{aligned} \quad (27)$$

In order to determine which of the nonlinear terms of (27) are nonzero we use the fact that the geometrical symmetry of the unperturbed system is  $O(2)$  and that the perturbation is small so that we can compute the projection integrals  $(A_n, A_j \bar{A}_k A_p)$  assuming that the modes  $A_n(x, y)$  are the modes of the system with full symmetry.

The (complex) 2-dimensional eigenspace for the linearisation of (27) at the first threshold, *i.e.* at the bifurcation point where the zero field solution loses its stability, must be a subspace of some particular isotypic component of the action of  $O(2)$  on the  $L_2$  function space  $\mathcal{H}$  spanned by the cavity modes (see [3, Theorem XII, 3.5] for example), and we can therefore assume that the modes  $A_n(x, y)$ , represented in polar coordinates  $(r, \psi)$  as  $A_n(r, \psi)$ , can be written as (complex) linear combinations of  $\cos(m\psi)$  and  $\sin(m\psi)$  for some  $m \in \mathbb{N}$ . If we suppose that the  $x$  and  $y$  axis are aligned with the symmetry axis of the perturbed system then we may take

$$A_1(r, \psi) = A_0(r) \cos(m\psi) \quad \text{and} \quad A_2(r, \psi) = A_0(r) \sin(m\psi), \quad (28)$$

where  $A_0(r)$  represents the radial profile of the two modes. The projection integrals in (27) have values

$$(A_n, A_j \bar{A}_k A_p) = \mathcal{M} \begin{cases} 3\pi/4 & n = j = k = p \\ \pi/4 & n = j \neq k = p \\ & \text{[all permutations of the} \\ & \text{four indices are allowed]} \\ 0 & \text{otherwise} \end{cases} \quad (29)$$



where the constant  $\mathcal{M}$  is given by

$$\mathcal{M} = \int_0^\infty A_0^2(r) \bar{A}_0^2(r) r dr. \quad (30)$$

Using (29) we can write (27) as

$$\begin{aligned} \frac{d}{dt} f_n &= \mu \left\{ \varepsilon - \mu^2 [\delta + (-1)^n \eta]^2 + i[\delta + (-1)^n \eta] \right\} f_n \\ &\quad - \frac{\mu \pi \mathcal{M}}{4(1 + \kappa)} \left[ (3|f_n|^2 + 2|f_p|^2) f_n + \bar{f}_n f_p^2 \right], \quad n = 1, 2, \quad p = 3 - n. \end{aligned} \quad (31)$$

To simplify the notation we scale time and the modal amplitudes by defining

$$\tau = \mu t, \quad \alpha_+ = \sqrt{\frac{\pi \mathcal{M}}{4(1 + \kappa)}} f_1, \quad \alpha_- = \sqrt{\frac{\pi \mathcal{M}}{4(1 + \kappa)}} f_2, \quad (32)$$

so that we can rewrite (31) as

$$\dot{\alpha}_+ = \left[ \varepsilon - \mu^2 (\delta - \eta)^2 + i(\delta - \eta) \right] \alpha_+ - \left( 3|\alpha_+|^2 + 2|\alpha_-|^2 \right) \alpha_+ - \bar{\alpha}_+ \alpha_-^2, \quad (33)$$

$$\dot{\alpha}_- = \left[ \varepsilon - \mu^2 (\delta + \eta)^2 + i(\delta + \eta) \right] \alpha_- - \left( 2|\alpha_+|^2 + 3|\alpha_-|^2 \right) \alpha_- - \alpha_+^2 \bar{\alpha}_-. \quad (34)$$

These are the expansions to third order of the equations (3–5) reduced to the centre manifold, and are the equations that we study for the remainder of this paper.

### 3.3 Symmetries

The system (33, 34) is unchanged by sign-reversal of either  $\alpha_+$  or  $\alpha_-$ , *i.e.* it is equivariant with respect to the symmetry group  $D_2 = Z_2(\sigma_x) \times Z_2(\sigma_y)$ , where we use the notation  $Z_r(\xi)$  to denote the cyclic group of order  $r$  generated by the element  $\xi$ . The actions of the group generators are:

$$\sigma_x : \begin{pmatrix} \alpha_+ \\ \alpha_- \end{pmatrix} \mapsto \begin{pmatrix} \alpha_+ \\ -\alpha_- \end{pmatrix}, \quad \sigma_y : \begin{pmatrix} \alpha_+ \\ \alpha_- \end{pmatrix} \mapsto \begin{pmatrix} -\alpha_+ \\ \alpha_- \end{pmatrix}, \quad (35)$$

and they represent the geometrical symmetries of the laser. Using (28) we see that, for example,  $\sigma_x$  corresponds to a reflection with respect to the  $x$ -axis: this leaves the cosine mode (amplitude  $\alpha_+$ ) unaltered and changes the sign of the sine mode (amplitude  $\alpha_-$ ).

The system (33, 34) is also equivariant with respect to the  $S^1$  action corresponding to global change of the phases of the two amplitudes:

$$R_\varphi : \begin{pmatrix} \alpha_+ \\ \alpha_- \end{pmatrix} \mapsto \begin{pmatrix} e^{i\varphi} \alpha_+ \\ e^{i\varphi} \alpha_- \end{pmatrix}. \quad (36)$$

In other words, the amplitudes  $\alpha_+$  and  $\alpha_-$  are defined only up to a common phase factor. Therefore the total symmetry of equations (33, 34) is the combination of the geometrical and the phase invariance symmetry. However, we note that we can write

$$\sigma_x = \sigma_y \circ R_\pi, \quad (37)$$

so the total symmetry group can be taken to be  $Z_2 \times S^1$ , where  $Z_2$  is generated by one of either  $\sigma_x$  or  $\sigma_y$ . The other geometrical symmetry can be obtained using (37). Therefore, the geometrical symmetry group  $D_2$  is recovered as a subgroup of  $Z_2 \times S^1$ .

We are now in a position to describe the bifurcation structure and interaction of the two modes following the extensive analysis in [14]. We summarise here the main results as they apply to our case. In the notation of [14] we have  $a = b = -1$  which places us on the lower boundary of region III(c) in Figure 4 of [14], from which the theoretical bifurcation diagrams can then be deduced using Figures 6 and 7 of [14]. In our Figure 1 we give versions of these diagrams as observed numerically in our context. The next subsection is devoted to explaining this Figure.

#### 3.4 The case $\delta \neq 0$ .

We consider first the case  $\delta > 0$ ; the results obtained are also valid for  $\delta < 0$  after exchanging  $\alpha_+$  with  $\bar{\alpha}_-$ . The important special case  $\delta = 0$  of cavity resonance, excluded from consideration in [14], will be discussed in the next subsection.

The phase invariance of (33) and (34) implied by the  $S^1$  symmetry makes the bifurcation analysis rather cumbersome. Therefore, it is convenient as in [14] to introduce the variables  $A$ ,  $\Phi$  and  $\Theta$  defined by:

$$v = A \cos(\Phi/2) e^{i\Theta_1}, \quad (38)$$

$$w = A \sin(\Phi/2) e^{i\Theta_2}, \quad (39)$$

$$\Theta = \Theta_1 + \Theta_2, \quad (40)$$

where

$$v = \alpha_+ - i\alpha_- \quad \text{and} \quad w = \bar{\alpha}_+ - i\bar{\alpha}_-. \quad (41)$$

We can reduce the two complex equations (33) and (34) to three real equations for  $A$ ,  $\Phi$  and  $\Theta$ :

$$\frac{dA}{dt} = \left[ \varepsilon - \mu^2 (\delta^2 + \eta^2) \right] A - \left[ 1 + \frac{1}{2} \sin^2 \Phi \right] A^3 + cA \sin \Phi \cos \Theta \cos \alpha \quad (42)$$

$$\frac{d\Phi}{dt} = -\frac{A^2}{2} \sin(2\Phi) + 2c [\cos \Theta \cos \alpha \cos \Phi - \sin \Theta \sin \alpha] \quad (43)$$

$$\frac{d\Theta}{dt} = -2\frac{c}{\sin \Phi} [\sin \Theta \cos \alpha + \cos \Theta \sin \alpha \cos \Phi] \quad (44)$$

(cf. [14]) where  $c$  is defined by

$$ce^{i\alpha} = \eta(2\mu^2\delta - i) \quad (45)$$

and plays the rôle of a (complex) symmetry breaking parameter in that it is zero if and only if the  $O(2)$  symmetry of the system is present. Note that in terms of  $A$ ,  $\Phi$  and  $\Theta$  both  $\sigma_x$  and  $\sigma_y$  have the same realisation

$$\sigma_x = \sigma_y = \sigma : \begin{pmatrix} A \\ \Phi \\ \Theta \end{pmatrix} \mapsto \begin{pmatrix} A \\ \pi - \Phi \\ -\Theta \end{pmatrix} \quad (46)$$

thus highlighting the fact that the symmetry of the problem can ultimately be considered to be  $Z_2$ , once the phase invariance  $S^1$  symmetry is factored out.

At  $\varepsilon = \varepsilon_1 \equiv \mu^2(\delta - \eta)^2$  the trivial solution  $\alpha_{\pm} = 0$  ( $A = \Theta = 0$ ,  $\Phi = \pi/2$ ) loses its stability through a Hopf bifurcation (bifurcation point  $P_1$  in Figure 1). A new nonzero single mode solution (standing wave solution  $SW$  in the notation of [14] and in Figure 1) with frequency

$$\omega_+ = \delta - \eta, \quad (47)$$

and amplitudes

$$|\alpha_+|^2 = \frac{1}{3} (\varepsilon - \mu^2\omega_+^2), \quad \alpha_- = 0 \quad (48)$$

appears and is stable. Note that in the context of equations (42–44) this bifurcation is a pitchfork and the new stable solution is stationary with values

$$A^2 = \frac{2}{3} (\varepsilon - \mu^2\omega_+^2), \quad \Phi = \pi/2, \quad \Theta = 0. \quad (49)$$

This simplification is a result of having factored out the  $S^1$  (phase invariance) group. The stationary point is a focus for

$$\varepsilon < \varepsilon_N \equiv 6\eta + \mu^2(\delta - \eta)^2 \quad (50)$$

and is a node otherwise.

There is an additional bifurcation from the zero solution. At  $\varepsilon = \varepsilon_6 \equiv \mu^2(\delta + \eta)^2$  there is a Hopf bifurcation to the unstable solution ( $SW_{\pi}$  in the notation of [14])

$$\alpha_+ = 0, \quad |\alpha_-|^2 = \frac{1}{3} [\varepsilon - \mu^2(\delta + \eta)^2]. \quad (51)$$

In terms of  $A$ ,  $\Phi$  and  $\Theta$  this is a pitchfork bifurcation to the unstable solution

$$A^2 = \frac{2}{3} [\varepsilon - \mu^2(\delta + \eta)^2], \quad \Phi = \pi/2, \quad \Theta = \pi. \quad (52)$$

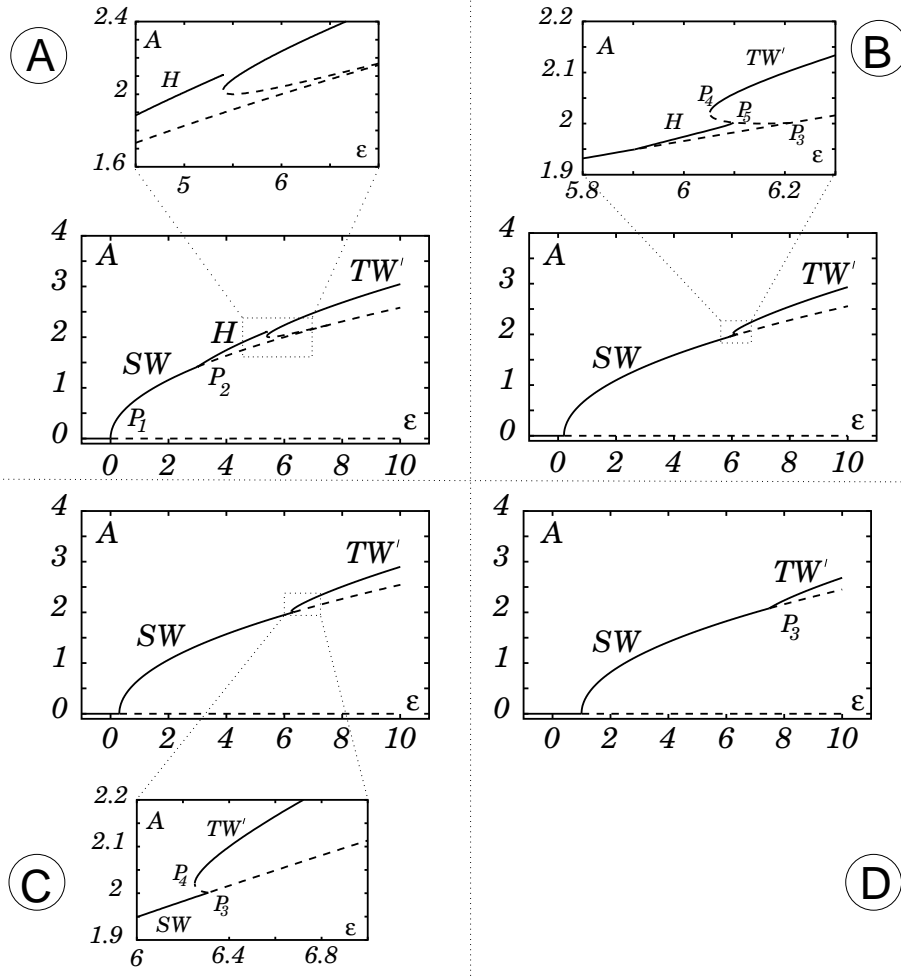


Fig. 1. *Bifurcation diagrams for  $\kappa = 1$  and  $\eta = 1$  (which imply that  $\delta_2 = 2$ ) and different values of the detuning parameter:  $\delta = \{1, 1.9, 2.1, 3\}$  from (A) to (D). The solid (dashed) lines correspond to stable (unstable) solutions. We have not drawn the unstable branch  $SW_\pi$ . The bifurcation points  $P_j$ ,  $j = 1, \dots, 5$  have horizontal coordinate  $\varepsilon_j$ . The vertical coordinate of the branches of stationary solutions is their amplitude  $A$ . That of the Hopf branch is the maximum of the amplitude during one period. For this reason in panel (A) the Hopf branch does not touch the limit point.*

There are no further bifurcations on this branch.

The  $SW$  branch may have a secondary Hopf bifurcation to a two-frequency solution (H in Figure 1) as the bifurcation parameter is increased to the value

$$\varepsilon_2 \equiv \mu^2 [(\delta + \eta)^2 + 8\delta\eta]. \quad (53)$$

This solution is characterised by both modes having non-zero amplitude, but different frequency so that beating between the two modes occurs.

As  $\delta$  tends to zero  $\varepsilon_2$  tends to  $\varepsilon_1$ , so that the secondary Hopf instability occurs closer and closer to the primary bifurcation from the trivial solution (see panel (A) in Figure 1).

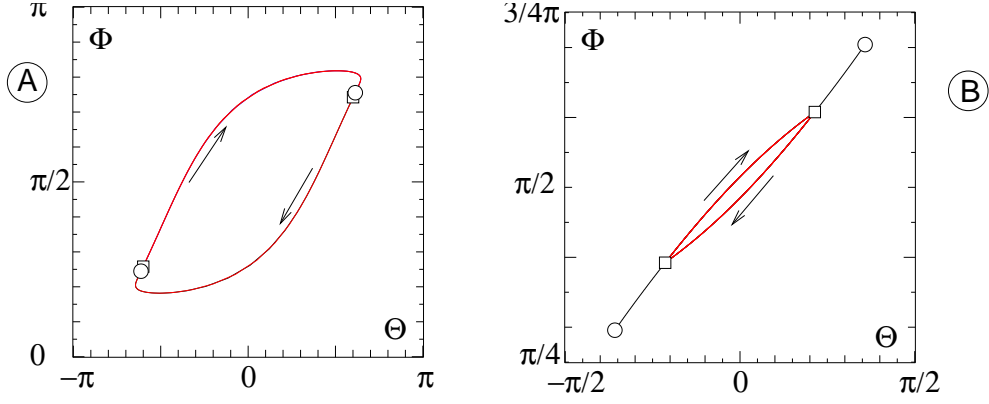


Fig. 2. (A) Blue sky bifurcation that ends the existence of the periodic orbit in panel (A) of Figure 1 at  $\varepsilon = 5.399$ . Two saddle node bifurcations (circle: stable fixed point, square: unstable fixed point) appear at symmetrical locations along the periodic orbit. (B) Disappearance of the periodic orbit in the case of panel (B) of Figure 1 at  $\varepsilon = 6.098$ . The periodic orbit clashes against the heteroclinic connections between the two unstable fixed points. All the parameters are as in Figure 1.

This secondary Hopf bifurcation point  $P_2$  exists only in the range

$$0 < \delta < \delta_2 \equiv \frac{1}{2\mu^2}. \quad (54)$$

In fact, another two stationary solutions appear at a third bifurcation point  $P_3$  on the SW branch, at

$$\varepsilon = \varepsilon_3 \equiv \frac{3\eta}{2\mu^2\delta} + \mu^2 [\eta^2 + \delta^2 + 4\delta\eta]. \quad (55)$$

In these solutions the two modes are frequency locked to each other and thus the intensity pattern is stationary.

If  $\delta = \delta_2$  then  $\varepsilon_2 = \varepsilon_3$  and the two bifurcation points  $P_2$  and  $P_3$  collide. The solutions that appear at  $P_3$  ( $TW'$  in Figure 1) have  $\alpha_+$  and  $\alpha_-$  both nonzero ( $\Phi \neq \pi/2$  and  $\Theta \neq 0$ ) and are interchanged by the symmetry operation  $\sigma$  defined by (46). The bifurcation is sub-critical if

$$0 \leq \delta \leq \delta_4 \equiv \sqrt{\frac{3}{2}}\delta_2, \quad (56)$$

(see panels (B) and (C) of Figure 1) and has a limit point  $P_4$  at

$$\varepsilon \equiv \varepsilon_4 = 2\sqrt{6}\eta + \mu^2(\eta^2 + \delta^2). \quad (57)$$

If  $\delta = \delta_4$  then  $\varepsilon_3 = \varepsilon_4$  and the limit point  $P_4$  hits the SW branch at  $P_3$ . For larger values of  $\delta$  the bifurcation is supercritical (see panel (D) of Figure 1).

The secondary Hopf branch ends either at  $P_4$  or, for larger values of  $\delta$ , at a point  $P_5$  on the the unstable branch that joins  $P_3$  and  $P_4$  (see panels (B) and (C) of Figure 1). In the former case the periodic orbit disappears in a blue sky bifurcation (panel (A) of Figure 2), that is the period tends to infinity until a saddle-node bifurcation creates a

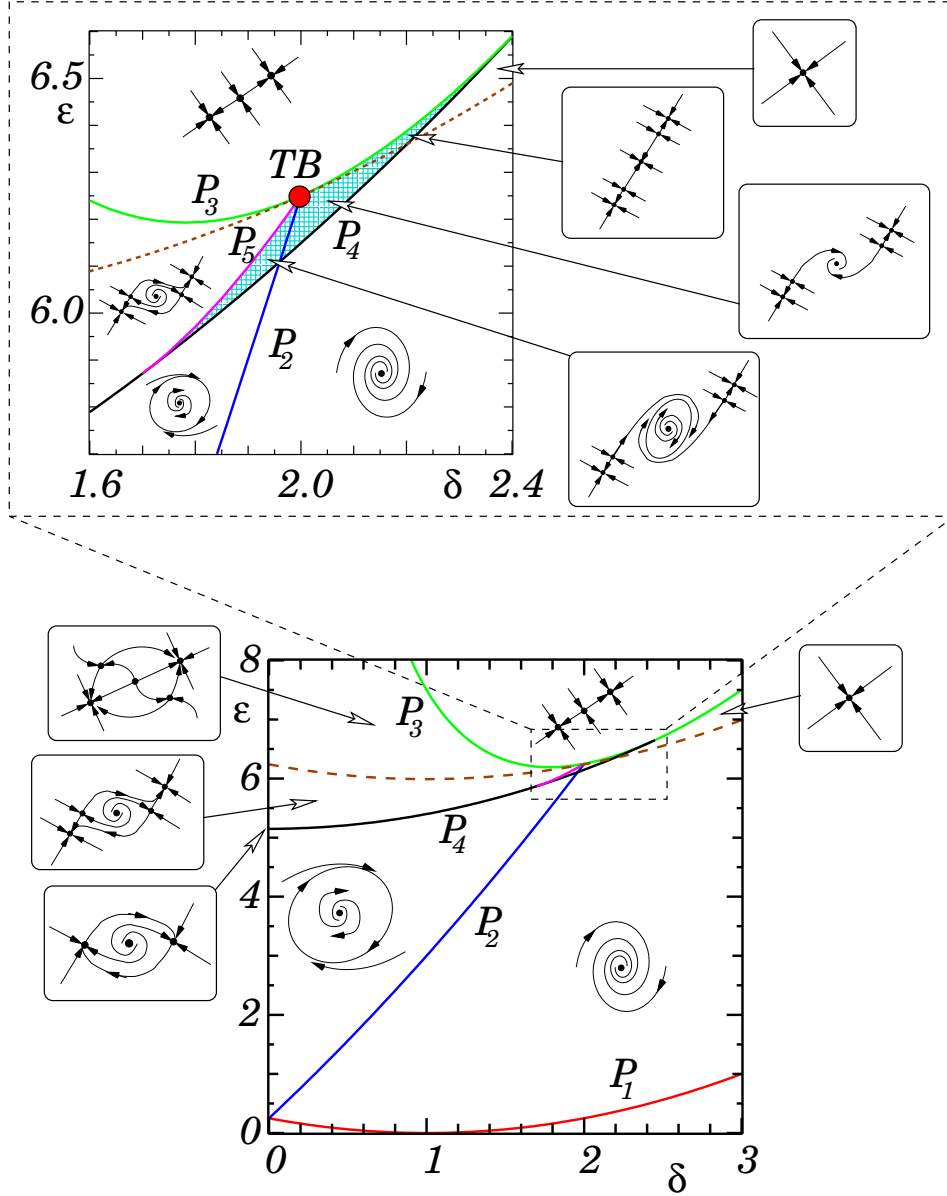


Fig. 3. State diagram of the equations (42–44) for  $\kappa = 1$  and  $\eta = 1$ . The line marked  $P_j$  represents the bifurcation point  $P_j$  of Figure 1 as a function of the parameters  $\epsilon$  and  $\delta$ . The dashed line represents the curve  $\epsilon_N$ : below it the SW point is a focus, above it is a node. The large dot next to the letters TB indicates the Takens-Bogdanov bifurcation point. The top part of the figure is an enlargement of the rectangular dashed section in the bottom part. The orbits drawn are just indicative of the type of dynamics expected in the corresponding parameter region and are not intended to be in any particular plane of the  $A$ ,  $\Phi$  and  $\Theta$  space.

sink and a saddle that ‘block’ the periodic orbit: compare [37, Fig.3]. In the latter case the period also tends to infinity, but the orbit collides with the heteroclinic orbits that join the unstable fixed points in the  $TW'$  branch (see panel (B) of Figure 2). There is no analytical expression for the coordinates of  $P_5$  and we have used AUTO [38,39] to plot it in Figure 1. Finally, note that even though the point  $P_3$  tends to infinity as  $\delta$  tends to zero,  $P_4$  is always finite: therefore the periodic orbit exists for only a finite range of values of  $\epsilon$ . These results are summarised in the state diagram in Figure 3.

The state diagram is organised around the bifurcation point of highest codimension (two), namely the  $Z_2$ -symmetric Takens-Bogdanov point (indicated by TB in Figure 3) which occurs when the points  $P_2$ ,  $P_3$  and  $P_5$  (see panels A and B of Figure 1) coincide, *i.e.* at  $\delta = \delta_2$ . In [14] the normal forms in the neighbourhood of this bifurcation point are derived as

$$\dot{\xi} = \eta + O(5), \tag{58}$$

$$\dot{\eta} = M_{TB}\xi^3 + N_{TB}\xi^2\eta + O(5), \tag{59}$$

in suitable coordinates  $\xi$  and  $\eta$ . The symbol  $O(5)$  represents terms of order at least five in  $\xi$  and  $\eta$  and the coefficients  $M_{TB}$  and  $N_{TB}$  depend on the parameters of equations (33, 34). The condition for a (non degenerate) Takens-Bogdanov singularity is  $M_{TB}N_{TB} \neq 0$ . Using the calculations given in Appendix A of [14] we find in our case  $M_{TB} = 1/3$  and  $N_{TB} = \mp 25/(18\sqrt{2})$ , where the signs refer respectively to the cases  $\delta > 0$  and  $\delta < 0$ . This implies that the bifurcation geometry in a neighbourhood of the Takens-Bogdanov point in Figure 3 is topologically equivalent to that obtained from a versal unfolding of a standard model as described for example in [18].

The bifurcation geometry in the neighbourhood of a  $Z_2$ -symmetric Takens-Bogdanov point is well documented: initial studies by Takens [40] with further analysis given by Carr [32], Guckenheimer and Holmes [41], Arnol'd [42], Khorozov [43] (see also [44]) and others show that a versal unfolding of the vector field at this singularity gives a bifurcation diagram determined by a smooth curve passing through the Takens-Bogdanov point and two rays emanating from it not tangent to the curve or each other (in contrast to the non-symmetric case). This is indeed the description of the bifurcation diagram in the neighbourhood of the point TB in Figure 3.

In applications, a Takens-Bogdanov bifurcation, whether symmetric or not, is often accompanied by additional characteristic features that arise from interaction with further equilibrium states. This can be seen, for example, in the forced van der Pol equation [45,46] (see also [41]) and in the dynamics of bulk liquid crystals in a shear flow [47]. The explanation for these accompanying patterns lies in the geometry of unfolding of a singularity of higher degeneracy and thus higher codimension: although it does not appear among the vector fields studied, its presence behind the scenes *organises* the configuration of lower codimension bifurcations. In the case of the van der Pol oscillator there is a triangular region in the neighbourhood of the (non symmetric) Takens-Bogdanov point (see Figure 2.1.2 of [41]) whose footprint can be recognised as part of the codimension-3 non symmetric bifurcations studied by Dumortier *et al.* [48].

An analogous phenomenon occurs here. The organising centre is a degenerate  $Z_2$ -symmetric Takens-Bogdanov singularity involving coalescence of *five* equilibrium states (instead of three for the non-symmetric case) and arising when  $M_{TB} = 0$  in equation (59). As in the van der Pol case, there is a ‘triangular’ region (shaded area in Figure 3) whose features are determined by the interactions of the five fixed points. However, we are not aware of a rigorous treatment of this case even though many authors have touched on aspects of it. For example, interactions of the five equilibria lead to interesting dynamical phenomena in certain fluid dynamical convection problems [12]. In the case of lasers, López-Ruiz *et al.* [33]

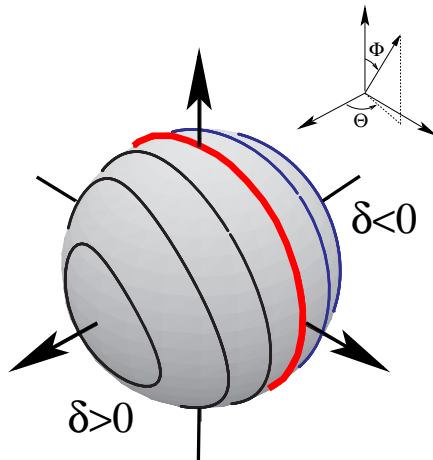


Fig. 4. Representation of the periodic orbits on the equations (42–44) in  $(\Theta, \Phi)$ -spherical coordinates for different values of the detuning parameter  $\delta$ . The orbits are contained in the nearer (further) hemisphere if  $\delta > 0$  ( $\delta < 0$ ). The limiting case  $\delta = 0$  corresponds to an orbit coinciding with a meridian of the sphere (thick line). In these simulations  $\kappa = 1$ ,  $\eta = 1$  and  $\delta = \{0.75, 0.50, 0.25, 0.00, -0.25, -0.50, -0.75\}$ .

give a bifurcation analysis only in the neighbourhood of the symmetric Takens-Bogdanov point. Krauskopf *et al.* [37,49,11,35] give spectacular and informative bifurcation diagrams away from the Takens-Bogdanov point, for a model that does not, however, involve the  $Z_2$ -symmetry. Rucklidge [13] considers bifurcations only near the Takens-Bogdanov point and with the sign of  $M_{TB}$  opposite to ours.

### 3.5 The case $\delta = 0$

#### 3.5.1 Introduction

If  $\delta = 0$  the symmetry-breaking parameter  $c$  defined by equation (45) is purely imaginary and equal to  $-i\eta$ . The physical interpretation is that from the point of view of the laser the modes are distinct because they have different resonant frequencies ( $\eta \neq 0$ ), but also there is no reason for the laser to choose one rather than the other as the pump parameter is increased through threshold. If instead  $\delta \neq 0$  then one mode has a lower threshold than the other, reflected in the fact that the symmetry-breaking parameter has a non-zero real part.

The solutions of equations (42–44) can be conveniently represented in spherical coordinates: the variable  $\Theta$  plays the rôle of the polar angle and the variable  $\Phi$  that of the azimuthal angle (see Figure 4). The two fixed points  $A \neq 0$ ,  $\Phi = \pi/2$  and  $\Theta = \{0, \pi\}$  correspond to diametrically opposed points in the equatorial plane and the periodic orbits are closed loops around them. Moreover, the sign of the detuning  $\delta$  determines in which hemisphere the periodic orbit is situated. The orbits for opposite values of  $\delta$  are related by the symmetry  $\sigma$  defined by (46).

If  $\delta = 0$  the orbit is constrained to the meridian  $\Theta = \pi/2$  that separates the two hemi-



spheres (see Figure 4) and thus has higher symmetry. This suggests in turn that the model may have an additional symmetry if  $\delta = 0$ . Therefore if we identify this additional symmetry we can use the tools of symmetric bifurcation theory [3,4] to analyse the  $\delta = 0$  case and its response to symmetry-breaking perturbations. This is the approach we follow throughout the rest of this section.

### 3.5.2 Additional discrete symmetry

As a first step we identify the symmetry group of the equations (33, 34) when  $\delta = 0$ . In this case the equations (33, 34) become

$$\begin{aligned}\dot{\alpha}_+ &= (\lambda - i\eta)\alpha_+ - (3|\alpha_+|^2 + 2|\alpha_-|^2)\alpha_+ - \bar{\alpha}_+\alpha_-^2 \\ \dot{\alpha}_- &= (\lambda + i\eta)\alpha_- - (2|\alpha_+|^2 + 3|\alpha_-|^2)\alpha_- - \bar{\alpha}_-\alpha_+^2\end{aligned}\tag{60}$$

where  $\lambda = \varepsilon - \mu^2\eta^2$ . Under the coordinate change (41) these correspond to the perturbed equations (2.7) of [14]

$$\begin{aligned}\dot{v} &= g(\lambda, |v|^2, |w|^2)v + c\bar{w} \\ \dot{w} &= \bar{g}(\lambda, |v|^2, |w|^2)w + \bar{c}v\end{aligned}\tag{61}$$

which have  $Z_2 \times S^1$  symmetry given by

$$\begin{pmatrix} v \\ w \end{pmatrix} \mapsto \begin{pmatrix} \bar{w} \\ \bar{v} \end{pmatrix} \quad \text{and} \quad \begin{pmatrix} v \\ w \end{pmatrix} \mapsto \begin{pmatrix} e^{i\varphi}v \\ e^{-i\varphi}w \end{pmatrix},\tag{62}$$

as shown earlier using equation (37). However, if  $\delta = 0$  the perturbation coefficient  $c$  is purely imaginary, and this case is excluded from consideration in [14]. Since  $g$  is real there is now an additional symmetry of order 2:

$$\tau : \begin{pmatrix} v \\ w \end{pmatrix} \mapsto -i \begin{pmatrix} \bar{v} \\ \bar{w} \end{pmatrix}\tag{63}$$

or, equivalently,

$$\tau : \begin{pmatrix} \alpha_+ \\ \alpha_- \end{pmatrix} \mapsto \begin{pmatrix} \bar{\alpha}_- \\ \bar{\alpha}_+ \end{pmatrix}.\tag{64}$$

Combined with the  $S^1$  action

$$R_\varphi : \begin{pmatrix} \alpha_+ \\ \alpha_- \end{pmatrix} \mapsto e^{i\varphi} \begin{pmatrix} \alpha_+ \\ \alpha_- \end{pmatrix}.\tag{65}$$

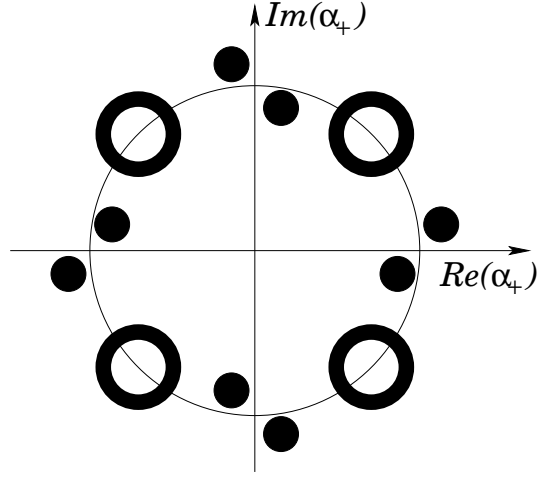


Fig. 5. Schematic representation of the intensity patterns in  $\text{Fix}(\Sigma_1)$ , equation (71). The black areas represent regions of high intensity. Their position along the thin circle indicates the corresponding value of the argument of  $\alpha_+$ .

this generates an action of  $O(2)$ . Moreover, the symmetry

$$\rho : \begin{pmatrix} \alpha_+ \\ \alpha_- \end{pmatrix} \mapsto \begin{pmatrix} i\alpha_+ \\ -i\alpha_- \end{pmatrix} \quad (66)$$

of order 4 commutes with both  $\tau$  and  $R_\varphi$ . This therefore gives as total symmetry group the subgroup  $Z_4 \times O(2)$  of the group  $S^1 \times O(2)$  generated by

$$P_\theta : \begin{pmatrix} \alpha_+ \\ \alpha_- \end{pmatrix} \mapsto \begin{pmatrix} e^{i\theta} \alpha_+ \\ e^{-i\theta} \alpha_- \end{pmatrix} \quad (67)$$

and  $O(2)$  as above. Notice that the  $S^1 \times O(2)$  action here corresponds to that in [14] under direct substitution of  $v, w$  in place of  $\alpha_+, \alpha_-$  although in our problem these coordinates are in fact related by (41). We shall return to this significant point later.

Observe that there is redundancy in the group action since the element  $\zeta = \rho^2 R_\pi$  acts trivially. Removing this redundancy yields the quotient group  $(Z_4 \times O(2))/Z_2(\zeta)$  which is cumbersome to work with both conceptually and notationally – in contrast to the  $(D_2 \times S^1)/Z_2(\sigma_x)$  case handled earlier which reduced simply to  $Z_2 \times S^1$ . We therefore prefer to focus on the group  $Z_4 \times O(2)$  with its transparent algebraic structure, while recognising that its *action* on  $\mathbb{C}^2 \cong \mathbb{R}^4$  is not faithful.

Once the symmetry group of the dynamical system has been established, we proceed to identify its subgroups and their fixed point spaces. The fixed point space  $\text{Fix}(\Sigma)$  of a given subgroup  $\Sigma$  is the vector space whose points are left unchanged by the action of  $\Sigma$ . The importance of fixed point spaces for bifurcation analysis is that they are invariant under the dynamics. In particular if  $\text{Fix}(\Sigma)$  is one-dimensional then typically at bifurcation there must be a branch of stationary solutions lying in  $\text{Fix}(\Sigma)$  (Equivariant Branching Lemma) and thus exhibiting the symmetries  $\Sigma$ . If  $\text{Fix}(\Sigma)$  is two-dimensional and the eigenvalues at bifurcation are purely imaginary then typically there is a branch of periodic solutions

lying in that subspace (Equivariant Hopf Theorem). See [3] or [4] for precise statements of these results.

The subgroups of  $Z_4 \times O(2)$  with 2-dimensional fixed point subspaces are found among those for  $S^1 \times O(2)$  (see [3]) and are (up to conjugacy) as follows:

$$\Sigma_1 : Z_2(\tau) \times Z_2(\rho^2 R_\pi), \quad \Sigma_2 : Z_4(\rho R_{-\frac{\pi}{2}}). \quad (68)$$

Their respective fixed point spaces are

$$\text{Fix}(\Sigma_1) = \left\{ \begin{pmatrix} \alpha_+ \\ \bar{\alpha}_+ \end{pmatrix} \right\}, \quad \text{Fix}(\Sigma_2) = \left\{ \begin{pmatrix} \alpha_+ \\ 0 \end{pmatrix} \right\}. \quad (69)$$

We next identify these fixed point spaces in terms of laser patterns. We know from equation (28) that  $\alpha_+$  and  $\alpha_-$  are the amplitudes of a cosine and sine mode respectively. In particular, for the purpose of this example we can assume that  $m = 1$  in (28) so that the expansion of the electric field can be written as

$$F(r, \psi, t) = \alpha_+(t)A_0(r) \cos(\psi) + \alpha_-(t)A_0(r) \sin(\psi). \quad (70)$$

The intensity pattern that corresponds to the elements of  $\text{Fix}(\Sigma_1)$  is

$$|F_{\text{Fix}(\Sigma_1)}|^2 = |A_0(r)|^2 |\alpha_+|^2 \{1 + \cos[2\arg(\alpha_+)] \sin(2\psi)\}. \quad (71)$$

As the argument of  $\alpha_+$  goes from 0 to  $2\pi$  the intensity pattern changes according to Figure 5. The elements of  $\text{Fix}(\Sigma_2)$  have an intensity pattern given by

$$|F_{\text{Fix}(\Sigma_2)}|^2 = |A_0(r)|^2 |\alpha_+|^2 \cos^2(\psi). \quad (72)$$

This corresponds to two bright spots aligned along the horizontal axis, independently of the phase of  $\alpha_+$ . There is also the corresponding sine pattern: this corresponds to  $\text{Fix}(\Sigma'_2)$  where  $\Sigma'_2$  is the conjugate  $\Sigma'_2 = \tau \Sigma_2 \tau^{-1}$  of  $\Sigma_2$ .

Given a stationary or periodic solution of a symmetric dynamical system we obtain other solutions by applying the elements of the symmetry group to it. It is important therefore, to understand how the full group  $Z_4 \times O(2)$  acts on the fixed point spaces  $\Sigma_1$  and  $\Sigma_2$ .

Let  $\alpha$  denote the vector  $(\alpha_+, \alpha_-)^T$ . If  $0 \neq \alpha \in \text{Fix}(\Sigma_1)$  then  $\rho\alpha \in \text{Fix}(\Sigma_1)$  as  $\rho$  commutes with  $\tau$ . On the other hand,  $R_\varphi\alpha \in \text{Fix}(\Sigma_1)$  just when  $\varphi = 0, \pi$ . Therefore the  $Z_4 \times O(2)$  orbit of  $\alpha$  consists of two circles intersecting  $\text{Fix}(\Sigma_1)$  at  $\{\alpha, -\alpha\}$  and  $\{\rho\alpha, -\rho\alpha\}$ . In physical terms this result means that if there is a solution in  $\text{Fix}(\Sigma_1)$ , then there are infinitely many copies of it, each obtained by multiplication by a phase factor. However, if the phase factor is equal to  $\pi$  then the net effect is not to obtain a different solution but to have moved half a period in  $\text{Fix}(\Sigma_1)$ .

If  $0 \neq \alpha \in \text{Fix}(\Sigma_2)$  then  $\rho\alpha \in \text{Fix}(\Sigma_2)$  and  $R_\varphi\alpha \in \text{Fix}(\Sigma_2)$  so the  $Z_4 \times O(2)$  orbit of  $\alpha$  consists of two circles  $C$  and  $\tau C$  lying in  $\text{Fix}(\Sigma_2)$  and  $\text{Fix}(\Sigma'_2)$  respectively. In other words, the net effect of the group action is to multiply a sine or cosine solution by a phase factor.

We can combine these results and make use of the Equivariant Hopf Theorem [3,4] to deduce the existence of branches of periodic solutions with these symmetries that bifurcate from the trivial solution.

**Theorem 1** *For the equations (60) there exist (at least) the following periodic solutions branching from the trivial solution as  $\lambda$  passes through zero:*

(1) *a family of solutions of the form*

$$W_\varphi(t) = \begin{pmatrix} r_\lambda e^{i\varphi} e^{i(\eta t + \theta)} \\ r_\lambda e^{i\varphi} e^{-i(\eta t + \theta)} \end{pmatrix}, \quad (73)$$

where  $r_\lambda \sim \lambda^{\frac{1}{2}}$  and  $\varphi$  and  $\theta$  are arbitrary. Here  $W_\varphi$  has reflection symmetry under  $R_\varphi \tau R_\varphi^{-1} = R_{2\varphi} \tau$  and a  $Z_4$  spatio-temporal symmetry under which increasing time by  $\pi/(2\eta)$  is equivalent to applying  $\rho$ ;

(2) *a pair of solutions of the form*

$$V_+, V_- = \begin{pmatrix} r_\lambda e^{i(\eta t + \theta)} \\ 0 \end{pmatrix}, \begin{pmatrix} 0 \\ r_\lambda e^{-i(\eta t + \theta)} \end{pmatrix} \quad (74)$$

respectively, where  $r_\lambda \sim \lambda^{\frac{1}{2}}$  and  $\theta$  is arbitrary. Each solution has spatio-temporal symmetry  $\widehat{SO}(2)$  given by shifting time by  $\Delta t$  and rotating by  $\theta = -\eta \Delta t$ .

Under time evolution the solution  $W_\varphi$  cycles across all the patterns in Figure 5. The solutions  $V_+$  and  $V_-$  correspond to the solutions  $SW$  and  $SW_\pi$ , equations (48) and (51). We will see below that for our particular system (60) these are the only solutions that branch from the trivial solution and, moreover, that the  $W_\varphi$  solution is stable and the  $V_\pm$  are unstable.

### 3.5.3 Disguised rotational symmetry

Interestingly as it turns out, the relations between the solutions for  $\delta = 0$  and those for  $\delta \neq 0$  described above can be elucidated by rewriting equations (60) in terms of new and somewhat artificial variables that restore to the equations a higher degree of symmetry. The linear terms of (60) commute with rotational symmetries

$$\begin{pmatrix} \alpha_+ \\ \alpha_- \end{pmatrix} \mapsto \begin{pmatrix} e^{i\varphi_1} \alpha_+ \\ e^{i\varphi_2} \alpha_- \end{pmatrix} \quad (75)$$

for arbitrary  $\varphi_1, \varphi_2$ , and so Takens' theory of normal forms [18] suggests the possibility of using a nonlinear coordinate change to remove (to any desired order) all nonlinear terms that do not share this symmetry. It is important to stress that the change of variables is nonlinear: although the linear transformation (41) removes the non- $O(2)$ -symmetric cubic terms  $\bar{\alpha}_+ \alpha_-^2$  and  $\alpha_+^2 \bar{\alpha}_-$  from equations (60), the linear terms in  $v$  and  $w$  in the resulting

equations (61) at the same time lose their full rotational symmetry. Normal form theory states that the nonlinear transformation will succeed when there are no *resonances* (that is, linear relations with integer coefficients) between the eigenvalues at the bifurcation point. In our case the eigenvalues at the bifurcation point are  $\pm i\eta$  and there are of course strong resonances, but careful inspection of the normal form method shows that the terms  $\bar{\alpha}_+\alpha_-^2$  and  $\bar{\alpha}_-\alpha_+^2$  can nevertheless be removed. To be precise:

**Theorem 2** *The nonlinear coordinate transformation*

$$\begin{pmatrix} \alpha_+ \\ \alpha_- \end{pmatrix} = \begin{pmatrix} \beta_+ \\ \beta_- \end{pmatrix} - \frac{1}{2\lambda + 4i\eta} \begin{pmatrix} \bar{\beta}_+\beta_-^2 \\ \bar{\beta}_-\beta_+^2 \end{pmatrix} \quad (76)$$

converts the equations (60) into

$$\begin{aligned} \dot{\beta}_+ &= (\lambda - i\eta)\beta_+ - (3|\beta_+|^2 + 2|\beta_-|^2)\beta_+ \\ \dot{\beta}_- &= (\lambda + i\eta)\beta_- - (2|\beta_+|^2 + 3|\beta_-|^2)\beta_- \end{aligned} \quad (77)$$

up to order 3.

*Proof.* Direct verification, or appeal to general theory [18] and the observation that it is the difference and not the sum of the eigenvalues  $\lambda \pm i\eta$  whose vanishing provides the obstruction to removing the non-rotational cubic terms.

Observe that the equations (77) have the form (61) with  $e = 0$  and with  $v, w$  corresponding to  $\beta_+, \beta_-$ , in contrast to the original correspondence defined by (76) and (41). Using the framework of [14] we can therefore express the symmetry as follows:

**Corollary 1** *After changing to  $\boldsymbol{\beta} \equiv (\beta_+, \beta_-)^T$  coordinates and truncating at order 3 the system (60) has  $S^1 \times O(2)$  symmetry with  $O(2)$  generated by  $\tau, R_\varphi$  and with  $S^1$ -action  $P_\theta$ .*

*Remark 1.* We recover the independent phase symmetries (75) by taking  $\varphi_1 = \varphi + \theta$  and  $\varphi_2 = \varphi - \theta$ .

*Remark 2.* If in (60) the two complex eigenvalues had been  $\lambda + i\eta$  (twice) rather than  $\lambda \pm i\eta$  then the equations would have  $D_4 \times S^1$  symmetry and (60) would already be in normal form: the terms  $(\bar{\alpha}_+\alpha_-^2, \bar{\alpha}_-\alpha_+^2)$  could not be removed. Compare [50], Sect.3.1.

*Remark 3.* We have been working with Taylor series truncations at order 3. In fact, normal form theory would allow us to transform away all those higher order terms in a full Taylor series extension of (60) that did not have  $S^1 \times O(2)$  symmetry. However, the higher the order the smaller the likely region of validity, and there is no guarantee that the system itself exhibits strict  $S^1 \times O(2)$  symmetry. This does not affect robust (structurally stable) features of the bifurcation scenario, but can affect sensitive features such as heteroclinic connections and families of orbits on an invariant torus. See [50] for a careful discussion of this issue for a system closely related to ours.

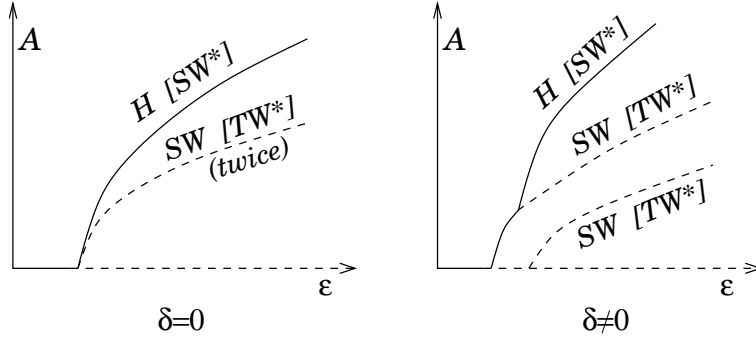


Fig. 6. Changes in the primary bifurcation point as  $\delta$  is increased from zero. The letters outside the brackets identify the branches with those in Figure 1 and refer to the equations in terms of  $\alpha_{\pm}$ . The letters in square brackets give the names of the branches as viewed in terms of the variables  $(v, w)$ .

The advantage of using the variables  $\beta$  is that we can now recast the problem of connecting the solutions for  $\delta = 0$  to those for  $\delta \neq 0$  as the problem of breaking the  $O(2)$  symmetry studied in [14]. There it is shown that the fully symmetric system has a standing wave solution  $v = \bar{w}$  and two travelling wave solutions  $(v, 0)$  and  $(0, w)$ . We indicate these standing and travelling wave solutions with the symbols  $SW^*$  and  $TW^*$  respectively. Translating in terms of  $\alpha_+$  and  $\alpha_-$  by identifying  $(v, w)$  with  $(\beta_+, \beta_-)$  and noting that

$$\alpha_+ = 0 \Leftrightarrow \beta_+ = 0, \quad \alpha_- = 0 \Leftrightarrow \beta_- = 0, \quad \bar{\alpha}_+ = \alpha_- \Leftrightarrow \bar{\beta}_+ = \beta_-, \quad (78)$$

we thus recover the results of Theorem 1 together with the additional information:

**Corollary 2** *The transformation  $\alpha \mapsto \beta$  converts the periodic solutions with  $Z_4$  spatio-temporal symmetry into rotationally symmetric ones, at least up to third order.*

In particular the Hopf solution  $W_{\varphi}$  (denoted by  $H$  in Figure 1) corresponds to  $SW^*$ , while the two solutions  $V_{\pm}$  ( $SW$  in Figure 1) correspond to the two solutions  $TW^*$ .

Furthermore, it is shown in [14] that as the real part of the symmetry breaking parameter  $e$  in equations (61) moves away from zero the two  $TW^*$  branches separate and the  $SW^*$  solution appears as a secondary bifurcation from one of the  $TW^*$  branches. In terms of the variables  $\alpha$  this implies that as  $\delta$  moves away from zero the two  $SW$  branches have different starting points, one at  $\varepsilon = \varepsilon_1$  the other at  $\varepsilon = \varepsilon_6$ . Moreover the Hopf branch becomes a secondary branch off the first  $SW$  branch. This is illustrated in Figure 6.

This picture is confirmed by standard bifurcation analysis for systems with two purely imaginary eigenvalues [18,41]. Using the  $\beta$  coordinates for both  $\delta$  zero and nonzero (but small) the parameters  $\varepsilon, \delta$  provide versal unfolding parameters about the organising centre  $(\varepsilon, \delta) = (\mu^2 \eta^2, 0)$ . In particular, we can see from Figure 7.5.2 of [41] (redrawn here in terms of  $\varepsilon$  and  $\delta$  as Figure 7) how the branching of the solutions  $W_{\varphi}$  and  $V_{\pm}$  that is simultaneous when  $\delta = 0$  changes when  $\delta \neq 0$ : a succession of two primary bifurcations with either  $\alpha_+ = 0$  or  $\alpha_- = 0$  is followed by a secondary (Hopf) bifurcation to a torus of periodic solutions. From (73) we also see that the period of these solutions is approximately given by  $2\pi/\eta$ .

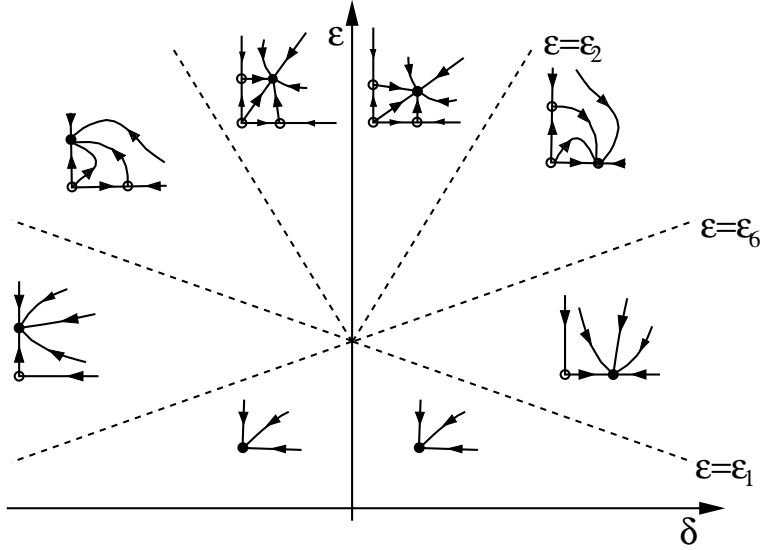


Fig. 7. Bifurcation set in the neighbourhood of  $(\varepsilon, \delta) = (\mu^2\eta^2, 0)$  in terms of the variables  $\beta_{\pm}$  (adapted from [41], Figure 7.5.2 case 1a). The axes of the small inserts are  $|\beta_{\pm}|$  and the filled and open circles indicate stable and unstable fixed points respectively.

To conclude the analysis of the bifurcation diagram for  $\delta = 0$  we note that the limit points of the  $TW'$  branches of panel A of Figure 1 exist for all sufficiently small  $|\delta|$  (including  $\delta = 0$ ). Exactly as in the case  $\delta \neq 0$  they are created at a symmetric pair of saddle-node bifurcations of periodic orbits that annihilate the torus (blue sky). These branches, found by direct calculation as in [14], are not connected to either of the  $\alpha_+ = 0, \alpha_- = 0$  branches when  $\delta = 0$  and so are not detectable by local bifurcation analysis in that case.

### 3.6 Numerical verification

In order to illustrate the range of applicability of the normal forms derived in this article we have integrated numerically the equations (3-5) that correspond to the cavity in Figure 8. The empty cavity modes can be expressed in terms of Hermite polynomials and are given by [51,52]:

$$A_{pq}(x, y, z) = \sqrt{\frac{2^{1-p-q}}{\pi w_x(z) w_y(z) p! q!}} H_p \left[ \frac{\sqrt{2}x}{w_x(z)} \right] H_q \left[ \frac{\sqrt{2}y}{w_y(z)} \right] e^{-x^2/w_x^2(z)} e^{-y^2/w_y^2(z)} \quad (79)$$

The indices  $p$  and  $q$  are nonnegative integers:  $p$  is the number of zeros of the field along the  $x$ -axis whilst  $q$  is the number of zeros along the  $y$ -axis. The functions  $w_x(z)$  and  $w_y(z)$  are  $z$  dependent scaling factors that represent the field beam waist, *i.e.* the spot size radius, along the  $x$  and  $y$  axis. They are functions respectively of  $R_x(\theta)$  and  $R_y(\theta)$  and are therefore different for all  $\theta \neq 0$ . For each value of  $z$  the cavity modes form an orthonormal basis for the space  $\mathcal{H}$ .

We have assumed that there are only two active modes,  $(p, q) = \{(1, 0), (0, 1)\}$ . The first mode is a ‘‘cosine’’ mode, *i.e.* its dependence on the polar angle  $\varphi$  is  $\cos(\varphi)$ , the second is a ‘‘sine’’ mode. In order to associate the solutions discussed in the previous section to

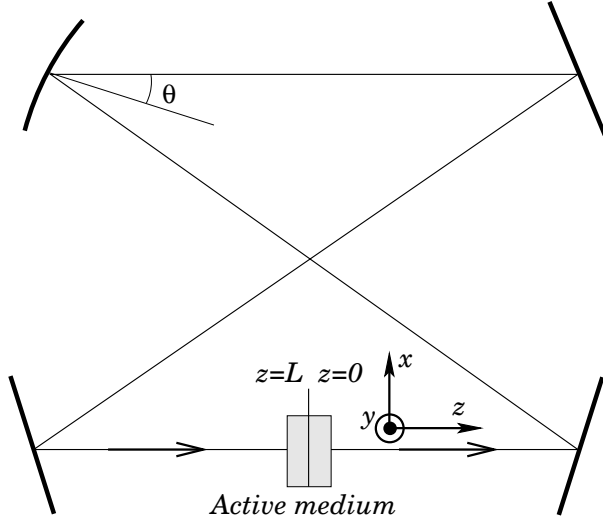


Fig. 8. Schematic diagram of a ring cavity laser. The  $z$  coordinate is along the cavity axis of length  $L$  and the points  $z = 0$  and  $z = L$  coincide.

laser patterns one should keep in mind that the intensity profiles of the cosine and sine mode consists of two bright spots aligned horizontally and vertically respectively.

The hypothesis that only two modes are active may not be realistic if the laser is operated well above threshold, but, on the other hand, the purpose of these simulations is to illustrate the application of the normal forms: these are only valid relatively close to threshold as they have been derived under the assumption that the field amplitudes are small.

We have scaled the longitudinal coordinate  $z$  and the radius of curvature of the mirror  $R$  to the cavity length  $L$ . The transverse dimensions  $x$  and  $y$  and the beam waists  $w_x(z)$  and  $w_y(z)$  are scaled to  $\sqrt{L\lambda/\pi}$ , where  $\lambda$  is the laser wave length. In these units the beam waists in the plane  $z = 0$  are given by [52]:

$$w_x \equiv w_x(0) = \left[ \frac{R \cos \theta}{2} - \frac{1}{4} \right]^{1/4}, \quad w_y \equiv w_y(0) = \left[ \frac{R}{2 \cos \theta} - \frac{1}{4} \right]^{1/4}. \quad (80)$$

The phase shift per cavity round-trip of the mode  $(p, q)$  is given by

$$\omega_{p,q} = \left( p + \frac{1}{2} \right) \omega_x + \left( q + \frac{1}{2} \right) \omega_y, \quad (81)$$

where

$$\omega_x = \arccos \left[ 1 - \frac{1}{R \cos \theta} \right], \quad \omega_y = \arccos \left[ 1 - \frac{\cos \theta}{R} \right], \quad (82)$$

so that the symmetry breaking parameter  $\eta$  used in (23) is given by

$$\eta = \frac{|\omega_x - \omega_y|}{2(1 - \mathcal{R})}, \quad (83)$$



where  $\mathcal{R}$  represents the total field reflectance of the cavity mirrors. The field decay rate  $\kappa$  is related to the mirror reflectance and the cavity round trip time  $T_c$  by

$$\kappa = \frac{1 - \mathcal{R}}{T_c}. \quad (84)$$

Finally, the scaling factor  $\mathcal{M}$  defined in (30) can be obtained by writing in polar coordinates in the plane  $z = 0$  the cavity modes  $A_{pq}$  given by equation (79) assuming that  $w_x = w_y$  (*i.e.* that the symmetry breaking is small enough for its effects to be neglected in the coefficients of the nonlinear terms). If we separate the radial and angular part and integrate them separately we obtain that

$$\mathcal{M} = \frac{2^6}{\pi^2 w_x^4} \int_0^\infty r^5 e^{-2r^2/w_x^2} dr = \frac{1}{\pi^2 w_x^2}. \quad (85)$$

We have chosen the values of the laser parameters in order to maximise the speed of integration:  $\gamma = 1$ ,  $\mathcal{R} = 0.97$ ,  $T_c = 0.03$  (hence  $\kappa = 1$ ). Finally, the radius of curvature of the mirror was set to  $R = 3/2$  and the angle  $\theta$  to  $\pi/32$  so that the symmetry breaking parameter is relatively small,  $\eta = 0.11377$ . We have simulated the case of one mode being in resonance with the atomic medium by selecting a value of the detuning equal to the mode frequency, that is  $\delta = \eta$ .

The program to integrate equations (3-5) represents the polarisation and population inversion on a rectangular grid thus transforming the partial differential equation into ordinary differential equations for the values of the fields at the grid points. These are integrated using a variable order variable step method [53]. The projection integral in equation (3) is computed using Gaussian quadrature [54].

We have run a set of simulations for different values of the pump parameter  $\chi = \kappa(1 + \varepsilon)$ . The results of these simulations are shown in Figure 9 overlaid on the bifurcation diagram of equations (33, 34). For small values of  $\varepsilon$  the agreement between the full equations and the predictions of the normal form is excellent. The laser switches on in a single mode stationary solution (see inset *SW* of Figure 9). This becomes unstable for larger pump values and a periodic orbit appears that oscillates between two patterns (see inset *H* of Figure 9). As the smallness parameter  $\varepsilon$  becomes larger the agreement between the normal forms and the full equations becomes worse. In both cases the periodic orbit disappears and is replaced by a stationary two mode solution (panel *TW'* in Figure 9), but the value of the pump parameter at which this happens is much larger for the full equations than for the normal forms. However, it is quite unlikely that only two modes of the laser would be active for these values of the pump parameter and is therefore debatable whether one should rely on the normal forms as a guide to the laser behaviour in this region of parameter space. Be that as it may, it is clear from the numerical simulations that the normal forms are an excellent vehicle for understanding the dynamics of a laser with broken symmetry both on a qualitative and quantitative level for values of the smallness parameter up to roughly 1/2.

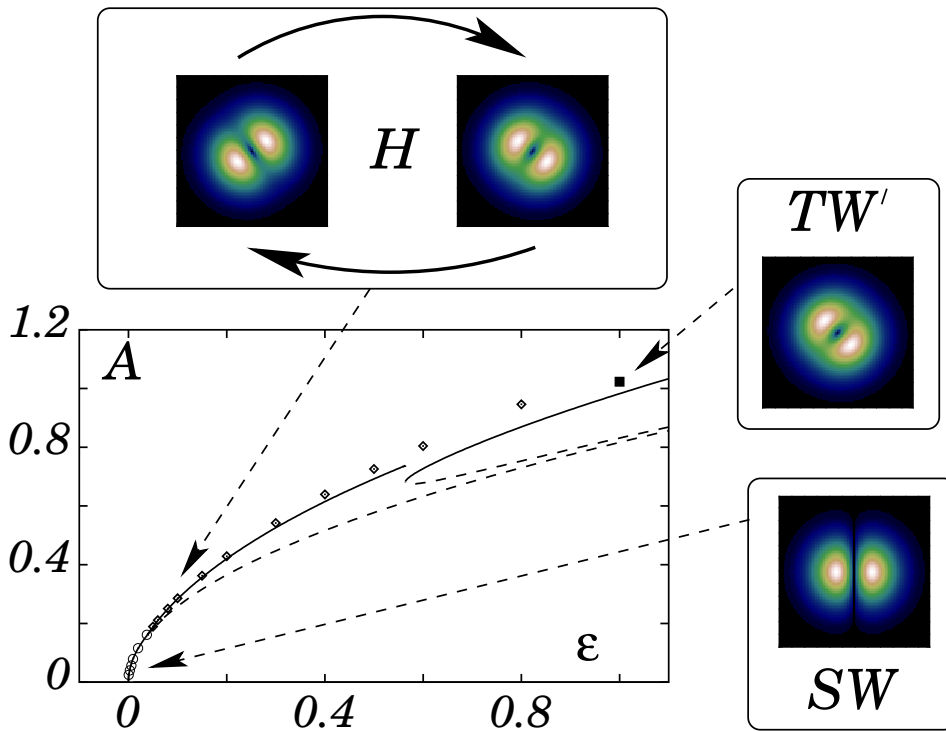


Fig. 9. Bifurcation diagram of equations (33, 34) for  $\kappa = 1$  and  $\eta = 0.11377$ ,  $\delta = \eta$ . The circles, diamonds and squares represent the results of numerical integration of the equations (3–5) for the cavity in Figure 8 using the parameters detailed in the text. The circles correspond to stationary single mode solutions (SW), the diamonds to periodic solutions (H) and the square represents a stationary two mode solution (TW'). The images in the inserts show the stationary field in the case of the SW and TW' solution and the two oscillating patterns in the case of the periodic solution.

#### 4 Conclusions

Normal forms have long been known as an extremely useful tool for studying the bifurcation structure of generic models derived solely on the basis of symmetry considerations. However, the connection between the parameters of a specific model and the coefficients of the corresponding normal forms is seldom made explicit in the bifurcation literature. In this paper we have addressed this issue for the case of a two level Maxwell-Bloch laser and have derived the formulae that express the coefficients of the normal forms in terms of the parameters of the laser. This is important for two reasons. On the one hand, we can identify the regions where the predictions derived from the normal forms are in quantitative agreement with the predictions of the full model in contrast to those where the agreement is only qualitative, as illustrated in Figure 9. On the other hand, we can clearly disentangle the “model-independent” features of a theory from the “model-dependent” features. Model-independent features are, for instance, the type of solutions and the bifurcations observed, which depend on the symmetry and on the first bifurcation and are, therefore, common to all models having the same symmetry and the same first bifurcation. Model-dependent features include the positions of the bifurcations and the widths of the stability windows in the control parameter space, and depend on important physical aspects of each individual model that do not affect the symmetry. In optics, for instance,

the number of energy levels included in the description of media interacting with light does not change the symmetry of the model. When more than one model is available, the ability to separate model-dependent and model-independent features is vital for ascertaining which model is the most accurate. In principle, this could be done by systematically comparing experiments and models over a wide range of control parameters. In practice, however, such checks are very difficult to carry out without a knowledge of where to look in parameter space for model-dependent features, since outside these regions all models with the same symmetry behave in much the same way.

In addition we have combined in this paper the analysis of two key bifurcation phenomena that apply to the Maxwell-Bloch laser and exhibited the relation between them in parameter space. Each of these phenomena has been well-studied in a variety of theoretical and applied contexts in the literature, but we are not aware of other studies that incorporate the full picture as we have presented it here. The curious interplay of travelling waves and standing waves is a new observation.

The role played by the symmetry generated by  $\tau$  at  $\delta = 0$  in organizing the bifurcations, as shown in Figure 6 and 7, is an important new result of section 3. From a physical point of view, this additional symmetry is present when the maximum of the gain profile  $\omega_A$  is between two cavity modes and these modes have the same gain. Up to the second order expansion of the gain line in small detunings, this happens for all active media. For large detunings, the gain profile needs to be symmetrical with respect to  $\omega_A$ , a condition verified in most lasers. We can conclude then that this symmetry is useful in understanding the interaction of two laser modes for a class of laser much larger than that described by the Maxwell-Bloch model used in this paper.

A final point worth remarking is that our derivation of the normal forms takes place in a broad context of breaking rotational symmetry. In this paper we have analysed in detail the case of an astigmatic laser, but the same normal forms could be used to study the symmetry breaking induced for example by the interaction of a metallic wave guide and an aperture, the case studied in [6,7].

## Acknowledgement

We thank Dr Philip Aston of the University of Surrey and Dr Alastair Rucklidge of the University of Leeds for several valuable discussions on symmetry-breaking issues.

## A Detailed calculations of the centre manifold expansion

At the heart of the centre manifold reduction [32] lies the splitting (18) of the fields  $\mathbf{u}$ . Let  $\mathbf{u}_{\parallel}$  denote the complex linear subspace of the function space  $\mathcal{H}$  generated by the active modes  $\mathbf{u}_n$ ,  $n \in \mathcal{J}$ . Centre manifold theory ensures that the local dynamics of equations (3-5) can be obtained by considering the restriction of the laser equations to the centre manifold of the trivial solution at bifurcation. On this manifold we can consider the non-active modes as functions of the active modes, that is  $\mathbf{u}_{\perp} = \mathbf{u}_{\perp}(\mathbf{u}_{\parallel})$ . The expression for the centre manifold is obtained by substituting this functional relation

into the laser equations (3-5). However, this is quite intractable unless we make some further simplifications. We therefore assume that we are sufficiently close to threshold so that the amplitudes of the active modes are small and we can approximate the centre manifold by the leading terms of its power series expansion in the amplitudes of the active modes.

In order to understand which terms of this series we need to compute it is convenient to write out in full the equation (20) for the amplitudes of the active modes:

$$\frac{d}{dt}f_n = \frac{1}{\mathcal{N}_n} \left( 1 + \lambda_n \begin{matrix} 1 & 0 \\ 0 & 1 \end{matrix} \right) \times \quad (\text{A.1})$$

$$\left( \begin{array}{l} - \sum_{p \in \mathcal{J}} \beta_p \frac{(1 + \lambda_p)}{\mathcal{N}_p} (A_n, A_p) f_p - (A_n, F_\perp) + \chi \sum_{p \in \mathcal{J}} \frac{(A_n, A_p)}{\mathcal{N}_p} f_p + (A_n, P_\perp) \\ - \chi \sum_{p \in \mathcal{J}} \frac{(A_n, A_p)}{\mathcal{N}_p} f_p - (A_n, P_\perp) + \\ \sum_{p \in \mathcal{J}} \frac{(1 + \lambda_p)}{\mathcal{N}_p} (A_n, (\chi + N) A_p) f_p + (A_n, (\chi + N) F_\perp) \\ - \gamma \left[ N - \frac{1}{2} (F \bar{P} + \bar{F} P) \right] \end{array} \right)$$

where the symbol  $(f, g)$  represents the  $L_2$  inner product of two functions  $f(x, y)$  and  $g(x, y)$ . Using the orthogonality relation (19), we can eliminate the terms linear in  $F_\perp$  and  $P_\perp$  in equation (A.1) and write it as

$$\begin{aligned} \frac{d}{dt}f_n &= \frac{1}{\mathcal{N}_n^2} \left[ \chi (1 + 2\lambda_n) - \beta_n (1 + \lambda_n)^2 \right] f_n \\ &\quad - \frac{1}{\mathcal{N}_n} \sum_{p \in \mathcal{J}} \frac{(1 + \lambda_p)}{\mathcal{N}_p} (A_n, N A_p) f_p + \frac{1}{\mathcal{N}_n} (A_n, N F_\perp) \\ &= \lambda_n f_n - \frac{1}{\mathcal{N}_n} \sum_{p \in \mathcal{J}} \frac{(1 + \lambda_p)}{\mathcal{N}_p} (A_n, N A_p) f_p + \frac{1}{\mathcal{N}_n} (A_n, N F_\perp), \quad n \in \mathcal{J}. \end{aligned} \quad (\text{A.2})$$

Inspection of equation (5) for the population inversion shows that it is at least of second order in the amplitudes of the active modes. This holds also for  $F_\perp$  since the source of the electric field is ultimately the term in  $N$  in the polarisation equation (4). Therefore the last two terms in (A.2) are respectively of third and fourth order in the amplitudes of the active modes. As we are interested only in a low order expansion of (A.2), we can drop the last term and expand the second term up to third order.

The lowest order terms in the expansion of the nonlinear terms on the right hand side of (5) are

$$\begin{aligned}
& \frac{1}{2} \left[ \sum_{j \in \mathcal{J}} \frac{(1 + \lambda_j) A_j}{\mathcal{N}_j} f_j \right] \left[ \chi \sum_{k \in \mathcal{J}} \frac{\bar{A}_k}{\bar{\mathcal{N}}_k} \bar{f}_k \right] + \text{c.c.} = \\
& \frac{1}{2} \sum_{j,k \in \mathcal{J}} \frac{(1 + \lambda_j) \chi}{\mathcal{N}_j \mathcal{N}_k} A_j \bar{A}_k f_j \bar{f}_k + \frac{1}{2} \sum_{j,k \in \mathcal{J}} \frac{(1 + \bar{\lambda}_j) \chi}{\bar{\mathcal{N}}_j \bar{\mathcal{N}}_k} \bar{A}_j A_k \bar{f}_j f_k = \\
& \sum_{j,k \in \mathcal{J}} \frac{[1 + (\lambda_j + \bar{\lambda}_k)/2]}{\mathcal{N}_j \bar{\mathcal{N}}_k} \chi A_j \bar{A}_k f_j \bar{f}_k. \tag{A.3}
\end{aligned}$$

This suggests expanding the population inversion as

$$N = \sum_{j,k \in \mathcal{J}} N_{jk} f_j \bar{f}_k \tag{A.4}$$

where the expansion coefficients  $N_{jk}$  are such that  $N_{jk} = \bar{N}_{kj}$  in order to ensure that  $N$  is real. Expressions for the  $N_{jk}$  can be obtained by substituting (A.4) into (5). Before doing so it is convenient to expand separately the left hand side of (5), *i.e.* to compute the time derivative of  $N$  in terms of the time derivative of the amplitudes of the active modes:

$$\frac{\partial N}{\partial t} = \sum_{j,k \in \mathcal{J}} N_{jk} \left( f_j \frac{d}{dt} \bar{f}_k + \bar{f}_k \frac{d}{dt} f_j \right). \tag{A.5}$$

Substituting the lowest order (*i.e.* the linear) terms of the active modes equation (A.2) into this expression we obtain

$$\frac{\partial N}{\partial t} = \sum_{j,k \in \mathcal{J}} (\lambda_j + \bar{\lambda}_k) N_{jk} f_j \bar{f}_k. \tag{A.6}$$

Substituting (A.6) and (A.3) into (5) we obtain

$$\sum_{j,k \in \mathcal{J}} (\lambda_j + \bar{\lambda}_k) N_{jk} f_j \bar{f}_k = -\gamma \sum_{j,k \in \mathcal{J}} \left\{ N_{jk} + \frac{[1 + (\lambda_j + \bar{\lambda}_k)/2]}{\mathcal{N}_j \bar{\mathcal{N}}_k} \chi A_j \bar{A}_k \right\} f_j \bar{f}_k, \tag{A.7}$$

from which we finally derive

$$N_{jk} = -\frac{1 + (\lambda_j + \bar{\lambda}_k)/2}{[1 + (\lambda_j + \bar{\lambda}_k)/\gamma] \mathcal{N}_j \bar{\mathcal{N}}_k} \chi A_j \bar{A}_k, \quad j, k \in \mathcal{J}. \tag{A.8}$$

Substituting this expression into the third term of (A.2) and keeping in mind that the last term of (A.2) can be neglected because it is of higher order we obtain the equation (21) for the amplitudes of the active modes.

## B Space dependent pump parameter

If the pump parameter is space-dependent the calculations to obtain the normal forms become much more involved. The principle behind the derivation remains unchanged, we still need to separate the slow from the fast modes, but its actual realisation is a non

trivial affair. If the pump is flat, *i.e.*  $\chi$  does not depend on the transverse coordinates, the cavity modes diagonalise the linear equations: therefore the slow modes are a subset of the cavity modes and we can relatively easily split the laser equations into two blocks. If the pump parameter is space dependent this is no longer true. The eigenmodes  $G_n(x, y)$  of the linearised laser equations (9) are no longer cavity modes, but can be expressed as linear superpositions of them:

$$G_n(x, y) = \sum_{k=1}^{\infty} g_k A_k(x, y). \quad (\text{B.1})$$

In order to separate the slow and fast dynamics we then need to project the equations (3-5) onto the modes  $G_n$  using the decomposition (B.1). This is of course possible in principle, but rather hard to do in practice, especially since the modes  $G_n(x, y)$  are usually only known numerically. Moreover, the laser equations are not diagonal on the basis of the modes  $G_n$  and the resulting equations for the amplitudes of these modes contain sums over all the coefficients  $\beta_n$  of equation (3). It is likely that a symbolic algebra package could be effective in splitting fast and slow variables, after which the procedure detailed in Appendix A can in principle be applied to obtain the normal forms.

## References

- [1] D.H. Sattinger, Group theoretic methods in bifurcation theory, Lecture notes in mathematics: 762, Springer-Verlag, Berlin, 1979.
- [2] M. Golubitsky, D.G. Schaeffer, Singularities and groups in bifurcation theory - Vol. I, Springer-Verlag, New York, 1985.
- [3] M. Golubitsky, I. Stewart, D.G. Schaeffer, Singularities and groups in bifurcation theory - Vol. II, Springer-Verlag, New York, 1988.
- [4] P. Chossat, R. Lauterbach, Methods in equivariant bifurcations and dynamical systems, World Scientific Pub., Singapore, 2000.
- [5] C. Green, G.B. Mindlin, E.J. D'Angelo, H.G. Solari, J.R. Tredicce, Spontaneous symmetry-breaking in a laser - the experimental side, Phys. Rev. Lett. 65 (1990) 3124–3127.
- [6] F. Papoff, G. D'Alessandro, W.J. Firth, G.-L. Oppo, Diffraction-induced polarization effects in optical pattern formation, Phys. Rev. Lett. 82 (1999) 2087–2091.
- [7] F. Papoff, G. D'Alessandro, G.-L. Oppo, Combined effects of polarization and non-paraxial propagation on pattern formation, Phys. Rev. A 60 (1999) 648–662.
- [8] F. Papoff, G. D'Alessandro, Pattern formation in lasers with Fabry-Pérot cavities and hard-edge diffraction, J.Opt. B: Quantum Semiclass. Opt. 2 (2000) 367–370.
- [9] E.J. D'Angelo, E. Izaguirre, G.B. Mindlin, G. Huyet, L. Gil, J.R. Tredicce, Spatiotemporal dynamics of lasers in the presence of an imperfect O(2) symmetry, Phys.Rev.Lett. 68 (25) (1992) 3702–3705.
- [10] R. López-Ruiz, G.B. Mindlin, C. Pérez-García, J.R. Tredicce, Mode-mode interaction for a CO<sub>2</sub> laser with imperfect O(2) symmetry, Phys.Rev.A 47 (1) (1993) 500–509.

- [11] B. Krauskopf, G.H.M. van Tartwijk, G.R. Gray, Symmetry properties of lasers subject to optical feedback, *Opt.Comm.* 177 (2000) 347–353.
- [12] L.N. Da Costa, E. Knobloch, N.O. Weiss, Oscillations in double-diffusive convection, *J. Fluid Mech.* 109 (1981) 25–43.
- [13] A.M. Rucklidge, Global bifurcations in the Takens-Bogdanov normal form with  $D_4$  symmetry near the  $O(2)$  limit, *Phys.Lett.A* 284 (2001) 99–111.
- [14] G. Dangelmayr, E. Knobloch, Hopf bifurcation with broken circular symmetry, *Nonlinearity* 4 (1991) 399–427.
- [15] L.A. Lugiato, L.M. Narducci, E.V. Eschenazi, D.K. Bandy, N.B. Abraham, Multimode instabilities in a homogeneously broadened laser, *Phys. Rev. A* 32 (3) (1985) 1563.
- [16] M. Golubitsky, I.N. Stewart, Hopf bifurcation in the presence of symmetry, *Arch. Rational Mech. Anal.* 87 (1985) 107–165.
- [17] M. Golubitsky, M. Roberts, A classification of degenerate Hopf bifurcations with  $O(2)$  symmetry, *J. Diff. Eqns.* 69 (1987) 216–264.
- [18] F. Takens, Singularities of vector fields, *Publ. Math. IHES* 43 (1974) 47–100.
- [19] J.R. Tredicce, A.M. Ghazzawi, C. Green, M.A. Pernigo, L.M. Narducci, L.A. Lugiato, Spatial and temporal instabilities in a  $CO_2$  laser, *Phys. Rev. Lett.* 62 (11) (1989) 1274–1277.
- [20] D. Dangoisse, D. Hennequin, C. Lepers, E. Louvergneaux, P. Glorieux, 2-dimensional optical lattices in a  $CO_2$  laser, *Phys. Rev. A* 46 (1992) 5955–5958.
- [21] E. Louvergneaux, D. Hennequin, D. Dangoisse, P. Glorieux, Transverse mode competition in a  $CO_2$  laser, *Phys. Rev. A* 53 (6) (1996) 4435–4438.
- [22] E. Louvergneaux, G. Sleky, D. Dangoisse, P. Glorieux, Coupled longitudinal and transverse self-organization in lasers induced by transverse-mode locking, *Phys. Rev. A* 57 (6) (1998) 4899–4904.
- [23] E. Louvergneaux, G. Sleky, D. Dangoisse, P. Glorieux, Spatial organization in a laser induced by phase locking of transverse modes, *Annales de Physique* 23 (SC1) (1998) 257–258.
- [24] A. Labate, R. Meucci, M. Ciofini, Polarization states of annular pattern in a nearly-isotropic laser resonator, *Opt. Comm.* 141 (3-4) (1997) 150–156.
- [25] M. Ciofini, A. Labate, R. Meucci, P.Y. Wang, Experimental evidence of selection and stabilization of spatial patterns in a  $CO_2$  laser by means of spatial perturbations, *Opt. Comm.* 154 (5-6) (1998) 307–312.
- [26] A.B. Coates, C.O. Weiss, C. Green, E.J. D’Angelo, J.R. Tredicce, M. Brambilla, M. Cattaneo, L.A. Lugiato, R. Pirovano, F. Prati, A.J. Kent, G-L. Oppo, Dynamical transverse laser patterns II. Experiments, *Phys. Rev. A* 49 (2) (1994) 1452–1466.
- [27] L.M. Narducci, J.R. Tredicce, L.A. Lugiato, N.B. Abraham, D.K. Bandy, Mode-mode competition and unstable behavior in a homogeneously broadened ring laser, *Phys. Rev. A* 33 (3) (1986) 1842–1854.
- [28] L.A. Lugiato, G.-L. Oppo, J.R. Tredicce, L.M. Narducci, M.A. Pernigo, Instabilities and spatial complexity in a laser, *J. Opt. Soc. Am. B* 7 (1990) 1019–1033.

- [29] H.G. Solari, R. Gilmore, Dynamics in the transverse section of the CO<sub>2</sub> laser, *J.Opt.Soc.Am.B* 7 (5) (1990) 828–841.
- [30] M. Brambilla, M. Cattaneo, L.A. Lugiato, R. Pirovano, F. Prati, A.J. Kent, G-L. Oppo, A.B. Coates, C.O. Weiss, C. Green, E.J. D’Angelo, J.R. Tredicce, Dynamical transverse laser patterns I. Theory, *Phys. Rev. A* 49 (2) (1994) 1427–51.
- [31] O. Svelto, Principles of lasers, 4th Edition, Plenum, New York, 1998.
- [32] J. Carr, Applications of Center Manifold Theory, Springer, Berlin, 1981.
- [33] R. López-Ruiz, G.B. Mindlin, C. Pérez-García, J.R. Tredicce, Nonlinear interaction of transverse modes in a CO<sub>2</sub> laser, *Phys.Rev.A* 49 (6) (1994) 4916–4921.
- [34] I. Boscolo, A. Bramati, M. Malvezzi, F. Prati, Three-mode rotating pattern in a CO<sub>2</sub> laser with high cylindrical symmetry, *Phys.Rev. A* 55 (1) (1997) 738–743.
- [35] C. Degen, B. Krauskopf, G. Jennemann, I. Fischer, W. Elsässer, Polarization selective symmetry breaking in the near-fields of vertical cavity emitting lasers, *J.Opt.B: Quantum Semiclass. Opt.* 2 (2000) 517–525.
- [36] A.G. Vladimirov, Bifurcation analysis of a bidirectional class B ring laser, *Opt. Comm.* 149 (1998) 67–72.
- [37] S. Wiczorek, B. Krauskopf, D. Lenstra, A unifying view of bifurcations in a semiconductor laser subject to optical injection, *Opt.Comm.* 172 (1999) 279–295.
- [38] E.J. Doedel, H.B. Keller, J.P. Kernévez, Numerical analysis and control of bifurcation problems: (I) Bifurcations in finite dimensions, *Int. J. Bifurcation and Chaos* 1 (3) (1991) 493–520.
- [39] E.J. Doedel, H.B. Keller, J.P. Kernévez, Numerical analysis and control of bifurcation problems: (II) Bifurcations in infinite dimensions, *Int. J. Bifurcation and Chaos* 1 (4) (1991) 745–772.
- [40] H.W. Broer, B. Krauskopf, G. Vegter (eds.), Global Analysis of Dynamical Systems (Floris Takens Festschrift), Institute of Physics Publishing, Bristol, 2001.
- [41] J. Guckenheimer, P.J. Holmes, Nonlinear oscillations, dynamical systems and bifurcations of vector fields, Springer-Verlag, New York, 1983.
- [42] V.I. Arnol’d, Geometric methods in the theory of ordinary differential equations, Springer-Verlag, New York, 1983.
- [43] E. Khorozov, Versal deformations of equivariant vector fields for the cases of symmetries of orders 2 and 3, *Topics in modern mathematics, Petrovskii Semin.* 5 (1985) 207–243.
- [44] V.I. Arnol’d (ed.), Dynamical Systems V - Encyclopaedia of Math. Sciences, Vol. 5, Springer-Verlag, Berlin, 1994.
- [45] A.W. Gillies, On the transformation of singularities and limit cycles of the variational equations of van der Pol, *Quart. J. Mech. Appl. Math.* 7 (1954) 152–167.
- [46] P.J. Holmes, D.A. Rand, Bifurcations of the forced van der Pol oscillator, *Quart. Appl. Math.* 35 (1978) 495–509.
- [47] E. Vicente-Alonso, PhD Thesis, University of Southampton, 2001.



- [48] F. Dumortier, R. Roussarie, J. Sotomayor, H. Żoładek, Bifurcations of planar vector fields, Lecture Notes in Math 1480, Springer-Verlag, Berlin, 1991.
- [49] S. Wieczorek, B. Krauskopf, D. Lenstra, Mechanisms for multistability in a semiconductor laser with optical injection, Opt.Comm. 183 (2000) 215–226.
- [50] J.W. Swift, Hopf bifurcation with the symmetry of the square, Nonlinearity 1 (1988) 333–377.
- [51] A.E. Siegman, Lasers, University Science, Mill Valley, California, USA, 1986.
- [52] Y.A. Anan'ev, Laser resonators and the beam divergence problem, Adam Hilger, Bristol, 1992.
- [53] Routine *ode* from the package *ode* of *netlib*: <http://www.netlib.org>
- [54] W.H. Press, S.A. Teukolsky, W.T. Vetterling, B.P. Flannery, Numerical Recipes in Fortran, 2nd Edition, Cambridge University Press, Cambridge, 1992.